

RESPONSES TO REVIEWERS

Response to Reviewer #1

We would like to thank the reviewer for the positive feedback. Below, we reply to the comments from the reviewer:

Comment 1: Section 3.1: Further discussions are desirable describing (and attributing) the model biases in terms of setup, errors in model meteorology, and processes included /excluded in different simulations.

Response: We have now included more detailed model descriptions regarding the chemistry and aerosol modules in the Materials and Methods section (Lines 152-170), along with an updated and extended Table 1 providing references to chemical mechanisms used in the models. In addition, we have also provided more discussion on possible model biases in section 3.1 (Lines 280-292), including some discussion on the meteorological biases. However, this paper does not aim to make a full evaluation and error attribution of the models. It does however build on Solazzo et al. (2017) in the same special issue that makes a deep evaluation of the models.

Comment: Page 10, l. 393-395: Why does SO₂ enhancement in case of reduced domestic emissions in North America are pronounced in a small belt over Europe? Is it possible to substantiate the statements with model simulated OH fields?

Response: We thank the reviewer for the careful review and we have identified a problem during the plotting. We have now corrected this plot. However, there is still a slight increase of SO₂ over the Alps that is simulated by the majority of the models. The AQMEII database unfortunately does not include OH fields so we cannot further evaluate this increase in this paper.

Comment: Page 4, l.162 – “where embedded” to “were embedded”

Response: Corrected (Line 184).

Comment: Page 7, l.276: “SO₂: : .by 35% 5”. Pl. check this sentence.

Response: Corrected (Line 305).

Comment: Page 7, l.279 – “effect” to “affects”

Response: Corrected (Line 308).

Response to Reviewer #2

We would like to thank the reviewer for the careful read of the manuscript positive feedback. Below, we reply to the comments from the reviewer:

Comment: - Table 1. You are ordering runs according to groups, not according to models. After a more thorough look many of the groups use the same model, sometimes even on the same resolution. What is the use of an ensemble of groups running the same model? Ideally this should give exactly the same results unless someone makes an error or the model version is different.

- Linked to the previous bullet: you end the conclusions with raising the issue of the impact of different model parameterization. However, you do not include such information. You should include a description of important model facts and add a discussion on these linking them to your results.

- Based on this information, perhaps some model runs should be removed from the ensemble (too many of the same model? Too simple parameterizations for some species?).

Response: We have now updated and extended Table 1, providing more information on the model specific spatial and vertical resolutions as well different chemistry and aerosol mechanisms. We have also added more information on the differences between the versions of the same models (e.g. CMAQ and WRF-Chem) by each group (Lines 152-170). The models or the versions of the same models differ from each and therefore, we think model removal is not necessary.

Comment: In the abstract you describe daily maximum 8h mean ozone. Is this what you show and evaluate in the tables and figures? Or is it monthly/annual means? You need to clarify this (in all figures/table legends as well as in the methods) or (/and) only include results in the abstract which you are actually showing as results in figures/tables.

Response: The model evaluation is based on monthly means, as described in the beginning of section 3.1. and the caption of Table 3 and the captions of Fig. 1 and 2. We have calculated the impact on daily maximum 8hr O₃ in order to show a policy impact of these reductions.

Comment: The RERER value analysis is interesting. It would be of great value if you describe the ozone RERER value based on monthly values (daily max 8h mean or mean), since ozone formation capacity/local contribution is seasonally dependent. Perhaps you can come up with a smart way of illustrating these rather than just adding more table values.

- I don't see the point of showing figures 11 (GLONAM-BAENAM) to 14 (EUREURBASEEUR). I would much rather see geographically resolved RERER values as a complement to the other figures.

Response: We thank the reviewer for his interest in the RERER analyses and we agree that it can be more emphasized in the paper. Therefore, we have now, as suggested by the reviewer, produced spatial distribution maps for O₃ and PM_{2.5} (Fig. 17) as well as monthly time series of the response for these pollutants (Fig 18) and added discussions on these results (Lines 578-606). On the other hand, we would like to keep Figs 11 and 14 to be consistent in the flow.

Comment: Line 221-224. The method of first taking difference then calculating mean is only valid if you are working with means. How do you treat the daily maximum 8h mean? Is the method valid for this metric (if that is what you are showing in the figures for ozone).

Response: The figures and tables only show the differences in monthly and annual means of the pollutants. Daily maximum 8hr ozone is only presented in the text as an additional information. As written in the text, we look at the difference in the mean of daily maximum 8hr ozone, but these are not presented in tables or figures.

Comment: Table 1. The number of simulations (scenarios) is different when comparing the table to the method text (for Europe). An x is missing in the table (grey area for north America-region).

Response: We thank the reviewer for the careful read. We have now corrected these.

Comment: Table 3. You state unit: % for NMB and NMGE, but the values in the table are clearly without unit. You should not have different units for North America and Europe (for RMSE in this case).

Response: We agree with the reviewer and we have now corrected the units in Table 3 caption.

Comment: You have a supplement but you do not refer to it in your manuscript.

Response: We thank the reviewer for pointing out this missing part. We have now referred to the supplement in various parts of the manuscript (Lines 194, 418-419, 520-521).

Comment: The figure legend of S3 is incorrect.

Response: We have now corrected the figure caption.

Comment: Section 2, first paragraph is messy and repetitive.

Response: We have now reorganized this paragraph (Lines 171-190).

1 **Influence of anthropogenic emissions and boundary conditions on multi-model**
2 **simulations of major air pollutants over Europe and North America in the framework**
3 **of AQMEII3**

4 Ulas Im¹, Jesper Heile Christensen¹, Camilla Geels¹, Kaj Mantzius Hansen¹, Jørgen Brandt¹,
5 Efisio Solazzo², Ummugulsum Alyuz³, Alessandra Balzarini⁴, Rocio Baro^{5,a}, Roberto
6 Bellasio⁶, Roberto Bianconi⁶, Johannes Bieser⁷, Augustin Colette⁸, Gabriele Curci^{9,10}, Aidan
7 Farrow¹¹, Johannes Flemming¹², Andrea Fraser¹³, Pedro Jimenez-Guerrero⁵, Nutthida
8 Kitwiroon¹⁴, Peng Liu¹⁵, Uarporn Nopmongkol¹⁶, Laura Palacios-Peña⁵, Guido Pirovano⁴,
9 Luca Pozzoli², Marje Prank^{17,18}, Rebecca Rose¹³, Ranjeet Sokhi¹¹, Paolo Tuccella^{9,10}, Alper
10 Unal³, Marta G. Vivanco^{8,19}, Greg Yarwood¹⁶, Christian Hogrefe²⁰, Stefano Galmarini²

11 ¹ Aarhus University, Department of Environmental Science, Frederiksborgvej 399, DK-4000,
12 Roskilde, Denmark.

13 ² European Commission, Joint Research Centre (JRC), Ispra (VA), Italy.

14 ³ Eurasia Institute of Earth Sciences, Istanbul Technical University, Istanbul, Turkey.

15 ⁴ Ricerca sul Sistema Energetico (RSE SpA), Milan, Italy.

16 ⁵ University of Murcia, Department of Physics, Physics of the Earth, Campus de Espinardo, Facultad
17 de Química, 30100 Murcia, Spain.

18 ⁶ Enviroware srl, Concorezzo, MB, Italy.

19 ⁷ Institute of Coastal Research, Chemistry Transport Modelling Group, Helmholtz-Zentrum
20 Geesthacht, Germany.

21 ⁸ INERIS, Institut National de l'Environnement Industriel et des Risques, Parc Alata, 60550 Verneuil-
22 en-Halatte, France.

23 ⁹ Dept. Physical and Chemical Sciences, University of L'Aquila, L'Aquila, Italy.

24 ¹⁰ Center of Excellence CETEMPS, University of L'Aquila, L'Aquila, Italy.

25 ¹¹ Centre for Atmospheric and Instrumentation Research (CAIR), University of Hertfordshire,
26 Hatfield, UK.

27 ¹² European Centre for Medium Range Weather Forecast (ECMWF), Reading, UK.

28 ¹³ Ricardo Energy & Environment, Gemini Building, Fermi Avenue, Harwell, Oxon, OX11 0QR, UK.

29 ¹⁴ Environmental Research Group, Kings' College London, London, UK.

30 ¹⁵ NRC Research Associate at Computational Exposure Division, National Exposure Research
31 Laboratory, Office of Research and Development, United States Environmental Protection Agency,
32 Research Triangle Park, NC, USA

33 ¹⁶ Ramboll Environ, 773 San Marin Drive, Suite 2115, Novato, CA 94998, USA.

34 ¹⁷ Finnish Meteorological Institute, Atmospheric Composition Research Unit, Helsinki, Finland.

35 ¹⁸ Cornell University, Department of Earth and Atmospheric Sciences, Ithaca, USA.

36 ¹⁹ CIEMAT, Avda. Complutense 40., 28040 Madrid, Spain.

37 ²⁰ Computational Exposure Division, National Exposure Research Laboratory, Office of Research and
38 Development, United States Environmental Protection Agency, Research Triangle Park, NC, USA.

39 ^a now at: Section Environmental Meteorology, Division Customer Service, ZAMG e Zentralanstalt für
40 Meteorologie und Geodynamik, 1190 Wien, Austria.

41

42 **Abstract**

43 In the framework of the third phase of the Air Quality Model Evaluation International
44 Initiative (AQMEII3), and as contribution to the second phase of the Hemispheric Transport
45 of Air Pollution (HTAP2) activities for Europe and North America, the impacts of a 20%
46 decrease of global and regional anthropogenic emissions on surface air pollutant levels in
47 2010 are simulated by an international community of regional scale air quality modeling

48 groups, using different state-of-the-art chemistry and transport models (CTM). The emission
49 perturbations at the global level, as well as over the HTAP2-defined regions of Europe, North
50 America and East Asia are first simulated by the global Composition Integrated Forecasting
51 System (C-IFS) model from European Centre for Medium-Range Weather Forecasts
52 (ECMWF), which provides boundary conditions to the various regional CTMs participating
53 in AQMEII3. On top of the perturbed boundary conditions, the regional CTMs used the same
54 set of perturbed emissions within the regional domain for the different perturbation scenarios
55 that introduce a 20% reduction of anthropogenic emissions globally as well as over the
56 HTAP2-defined regions of Europe, North America and East Asia.

57 Results show that the largest impacts over both domains are simulated in response to the
58 global emission perturbation, mainly due to the impact of domestic emissions reductions. The
59 responses of NO₂, SO₂ and PM concentrations to a 20% percent anthropogenic emission
60 reductions are almost linear (~20% decrease) within the global perturbation scenario with
61 however, large differences in the geographical distribution of the effect. NO₂, CO and SO₂
62 levels are strongly affected over the emission hot spots. O₃ levels generally decrease in all
63 scenarios by up to ~1% over Europe, with increases over the hot spot regions, in particular in
64 the Benelux region, by an increase up to ~6% due to the reduced effect of NO_x-titration. O₃
65 daily maximum of 8-hour running average decreases in all scenarios over Europe, by up to
66 ~1%. Over the North American domain, the central-to-eastern part and the western coast of
67 the U.S experience the largest response to emission perturbations. Similar but slightly smaller
68 responses are found when domestic emissions are reduced. The impact of inter-continental
69 transport is relatively small over both domains, however, still noticeable particularly close to
70 the boundaries. The impact is noticeable up to a few percent, for the western parts of the
71 North American domain in response to the emission reductions over East Asia. O₃ daily
72 maximum of 8-hour running average decreases in all scenarios over North Europe by up to
73 ~5%. Much larger reductions are calculated over North America compared to Europe.

74 In addition, values of the Response to Extra-Regional Emission Reductions (RERER) metric
75 have been calculated in order to quantify the differences in the strengths of non-local source
76 contributions to different species among the different models. We found large RERER values
77 for O₃ (~0.8) over both Europe and North America, indicating a large contribution from non-
78 local sources, while for other pollutants including particles, low RERER values reflect a
79 predominant control by local sources. [A distinct seasonal variation in the local vs. non-local
80 contributions has been found for both O₃ and PM_{2.5}, particularly reflecting the spring-time
81 long-range transport to both continents.](#)

Formatted: Subscript

Formatted: Subscript

82 1. Introduction

83 Regional air quality modeling has considerably developed during recent decades, driven by
84 increased concern regarding the impact of air pollution on human health and ecosystems.
85 Numerous air quality models have been developed by research groups worldwide and are
86 being widely used for developing and testing emission control policies. Regional atmospheric
87 chemistry and transport models (CTMs) are widely used to assess the past, present and future
88 levels of air pollutants from continental to regional scales. There are different sources of

89 uncertainties in models such as emissions, meteorology, boundary conditions and chemical
90 schemes that should be taken into account when analyzing results. These uncertainties
91 become more critical when these models are used for regulatory applications such as impacts
92 of emission reductions. Multi-model ensembles can help in reducing this uncertainty and
93 provide a better estimate of impacts under different scenarios (Solazzo et al., 2013; Galmarini
94 et al., 2013; Kioutsoukis et al., 2017).

95 Numerous observational and modeling studies show that long-range transport of pollutants
96 degrade air quality over remote continents (e.g., Wilkening et al., 2000; Holloway et al.,
97 2003; Akimoto, 2003; Fiore et al., 2009). Although the influence of foreign emissions on
98 continental scales is seen most frequently in the free troposphere, surface levels can also be
99 affected, in particular over locations that generally receive clean air masses (e.g. Li et al.,
100 2002). For example, dust storms and biomass burning can influence the tropospheric
101 composition on a hemispheric scale (e.g., Husar et al., 2001; Jaffe et al., 2004). Reducing air
102 pollution levels in surface air would improve public health as exposure to these atmospheric
103 constituents aggravates respiratory illness and leads to premature mortality (World Health
104 Organization, 2013; Im et al., 2017; Liang et al., 2017). However, attributing pollution to
105 specific source regions is complicated due to the different processes influencing
106 intercontinental transport and by a large hemispheric background and the dominance of local
107 emissions in contributing to high levels of particular pollutants, such as ozone (O₃) (e.g. Fiore
108 et al., 2009). Given these difficulties, estimates of source-receptor relationships rely heavily
109 on models.

110 Stjern et al. (2016), using ten models participating in the second Hemispheric Transport of
111 Air Pollution (HTAP2) activity, showed that a 20% reduction of global anthropogenic
112 emissions, leads to significant changes regionally. They found that for North America (NA),
113 black carbon emissions controls in East Asia are more important than domestic mitigation. In
114 the framework of the HTAP2 activity, UN (2007) showed that a 20% reduction of North
115 American NO_x emissions leads to a 0.22 ppb decrease in O₃ levels over Europe (EU), while a
116 20% decrease in East Asian NO_x emissions leads to a decrease of North American surface O₃
117 levels by 0.12 ppb. The impacts of these emissions changes on the O₃ levels in the source
118 regions are much higher. The impact of lateral boundary conditions (LBC) on concentration
119 fields simulated by regional-scale air quality models can also be quite significant (Jimenez et
120 al., 2007; Mathur, 2008; Rudich et al., 2008; Song et al., 2008; Anderrson et al., 2015;
121 Giordano et al., 2015, Hogrefe et al., 2017; Solazzo et al., 2017a). Recently, Giordano et al.
122 (2015) showed that the regional models can be very sensitive to the boundary conditions
123 provided by the global models. Tang et al. (2007) showed that the simulated surface levels
124 over polluted areas are usually not as sensitive to the variation of LBCs, but are more
125 sensitive to the magnitude of their background concentrations. Jonson et al. (2017), in the
126 framework of the HTAP2 activity, showed that for ozone the contributions from the rest of
127 the world is larger than the effects from European emissions alone, with the largest
128 contributions from North America and East Asia. The majority of these studies that address
129 impact of emissions on regional and inter-continental transport employ global models on
130 coarse spatial resolution or focus on just a few species, such as O₃ or carbon monoxide (CO).

131 On the other hand, studies using regional chemistry and transport models at finer spatial
132 resolutions mostly focus on sub-regional scales (e.g. Im and Kanakidou, 2012; Huszar et al.,
133 2016). Therefore, studies addressing multi-pollutant, source-receptor relationships on inter-
134 continental and regional scales can provide valuable information on the impact of domestic
135 and foreign emissions on regional air pollution levels. Multi-model ensembles operating on
136 fine spatial resolutions can increase accuracy and provide an estimate of uncertainty.

137 The Air Quality Model Evaluation International Initiative (AQMEII), coordinated jointly by
138 European Commission, Joint Research Centre (EC-JRC) and the U.S. Environmental
139 Protection Agency (EPA) has brought together regional chemistry and transport modelling
140 groups from Europe and North America since 2008 (Rao et al., 2012; Solazzo et al., 2012a,b;
141 Im et al., 2015 a,b). AQMEII is now running its third phase as a regional sub-project of the
142 larger Hemispheric Transport of Air Pollution (HTAP), which in turn is a taskforce of Long
143 Range Transport of Air Pollution program (LTRAP) of United Nations Economic
144 Commission for Europe (UNECE) (Galmarini et al., 2017). The aim of the study is to assess
145 the impact of global and HTAP2-defined regional anthropogenic emission reductions of 20%
146 in Europe, North America and East Asia on major air pollutant levels over Europe and North
147 America using a multi-model ensemble approach. The study will also investigate the local vs.
148 non-local contributions to different air pollutant levels, adopting the Response to Extra-
149 Regional Emission Reductions (RERER) metric developed by the HTAP2 community
150 (Galmarini et al., 2017).

151 2. Materials and Methods

152 In the framework of the AQMEII3 project, ~~fourteen~~^{twelve} groups contributed to the
153 simulation of the air pollution levels for 2010 in Europe (EU) and three groups for North
154 America (NA) ~~in the year 2010~~ (Table 1 and Solazzo et al., 2017b). As seen in Table 1,
155 different groups used same CTM models, such as the CMAQ and WRF-Chem model. The
156 main differences among these models reside in the number of vertical levels, horizontal
157 spacing, biogenic emissions, gas/aerosol modules in the models and the model releases
158 (Table 1). For example, regarding groups that used the CMAQ model, UK1, DE1 and US3
159 calculated biogenic emissions using the BEIS (Biogenic Emission Inventory System version
160 3) model, while TR1, UK1 and UK2 calculated biogenic emissions through the Model of
161 Emissions of Gases and Aerosols from Nature (MEGAN) (Guenther et al., 2012). Moreover,
162 DE1 does not include the dust module, while the other CMAQ instances use the inline
163 calculation (Appel et al., 2013), and TR1 uses the dust calculation previously calculated for
164 AQMEII phase 2. Finally, all runs were carried out using CMAQ version 5.0.2, except for
165 TR1, which is based on the 4.7.1 version. The gas-phase mechanisms and the aerosol models
166 used by each group are also presented in Table 1. IT1 used the WRF-Chem model version
167 3.6, with a new chemistry that includes a better representation of the secondary organic
168 aerosol mass in the simulation of direct and indirect aerosol effects (Tuccella et al., 2015). In
169 addition, only direct effects were included in the IT1 simulation. ES1 model also used WRF-
170 Chem, with different gas phase chemistry. More details of the model system are provided in
171 the supplementary material in Im et al. (2018).

172 The emission inventories that are used in the second phase of AQMEII for Europe and North
173 America (Im et al., 2015a,b) and extensively described in Pouliot et al. (2015) are also used
174 in AQMEII3. For the EU, the 2009 ~~anthropogenic emission~~ inventory ~~offrom the Monitoring~~
175 ~~Atmospheric Composition & Climate (MACC) anthropogenic emissions~~ was used. ~~In regions~~
176 ~~not covered by the Monitoring Atmospheric Composition & Climate (MACC) inventory,~~
177 ~~such as North Africa, five modelling systems have complemented the standard inventory with~~
178 ~~the HTAPv2.2 datasets (Janssens-Maenhout et al., 2015).~~ For the NA domain, the 2008
179 National Emissions Inventory was used ~~as the basis for the 2010 emissions~~ with 2010-
180 specific adjustments for major point sources, mobile sources and wildfires (Pouliot et al.,
181 2015). The emissions were then treated with the SMOKE emissions processing system
182 (Mason et al., 2012). ~~For both continents, the regional scale emission inventories were~~
183 ~~embedded in the global scale inventory (Janssens-Maenhout et al., 2015) to guarantee~~
184 ~~coherence and harmonization of the information used by the regional and global scale~~
185 ~~modelling communities (Galmarini et al., 2017).~~ The majority of the European groups used
186 MACC emissions over Europe, while FII and FRES1 supplemented the MACC emissions
187 with HTAP emissions over North Africa (Table 1). For NA, the temporal and vertical
188 allocation of emissions vary between the groups that used the "SMOKE" files (DE1, US1,
189 US3) and the gridded HTAP files (DK1), however the annual total mass are exactly the same.
190 ~~In order to guarantee consistency between the groups using the regional scale MACC or~~
191 ~~SMOKE emissions, and the groups using the HTAPv2.2 emissions, the regional scale~~
192 ~~emission inventories were embedded in the HTAPv2.2 inventory (Janssens-Maenhout et al.,~~
193 ~~2015;) to Galmarini et al., 2017).~~ Overall, there was a high level of harmonization of
194 emission inputs even if there were some differences in how they were adapted by each
195 modeling group for their system. Chemical boundary conditions for both domains were
196 provided by the European Center for Medium Range Weather Forecasts (ECMWF)
197 Composition – Integrated Forecast System (C-IFS) model (Flemming et al., 2015)

198 2.1. Emission perturbations

199 The perturbation scenarios feature a reduction of 20% of the anthropogenic emissions
200 globally and in HTAP-defined regions of Europe, North America and East Asia (Table 2 ~~and~~
201 ~~Fig. S1~~). The choice of 20% was motivated by the consideration that the perturbation would
202 be large enough to produce a sizeable impact (i.e. more than numerical noise) even at long
203 distances while small enough to be in the near-linear atmospheric chemistry regime
204 (Galmarini et al., 2017). The emission reductions are implemented in both the global C-IFS
205 model that provides the boundary conditions to the participating regional models, as well as
206 in the regional models. The regional models use the corresponding set of boundary conditions
207 extracted from the C-IFS model. Among the fourteen groups that participated to the
208 AQMEII3 base case simulations, twelve groups from Europe and two groups from North
209 America simulated at least one of the three emission perturbation scenarios, shown in Table
210 1. Two of the European groups (DE1 and DK1) also simulated the base and the three
211 perturbation scenarios for the North American domain.

- 212 - The global perturbation scenario (GLO) reduces the global anthropogenic emissions
213 by 20%. This change has been implemented in the C-IFS global model that provides

214 the boundary conditions to the regional models participating in the AQMEII
215 ensemble. Therefore, the GLO scenario introduces a change in the boundary
216 conditions as well as a 20% decrease in the anthropogenic emissions used by the
217 regional models. Nine groups over the EU domain and four groups over the NA
218 domain have simulated the GLO scenario.

- 219 - The North American perturbation scenario (NAM) reduces the anthropogenic
220 emissions in North America by 20%. This change has been implemented in the C-IFS
221 global model that provides the boundary conditions to the regional models used in the
222 AQMEII ensemble. Therefore, the NAM scenario introduces a change in the
223 boundary conditions while anthropogenic emissions remain unchanged for Europe,
224 showing the impact of long-range transport of North American pollutants to Europe
225 while for North America, the scenario introduces a 20% reduction of anthropogenic
226 emissions in the HTAP-defined North American region, showing the contribution
227 from the domestic anthropogenic emissions. Seven groups over the EU domain and
228 three groups over the NA domain have simulated the NAM scenario.
- 229 - The European perturbation scenario (EUR) reduces the anthropogenic emissions in
230 the HTAP-defined Europe domain by 20%. The EUR scenario introduces a change in
231 the anthropogenic emissions over the EUR region in the CTMs, showing the
232 contribution from the domestic anthropogenic emissions. Six groups have simulated
233 the EUR scenario over the EU domain.
- 234 - The East Asian perturbation scenario (EAS) reduces the anthropogenic emissions in
235 East Asia by 20%. Similar to the NAM scenario for the EU domain, the EAS scenario
236 introduces a change in the boundary conditions while anthropogenic emissions remain
237 unchanged in the regional models, showing the impact of long-range transport from
238 East Asia on the NA concentrations. Four groups have simulated the EAS scenario
239 over the NA domain.

240 In AQMEII, all participating groups were required to upload modelled hourly surface
241 concentrations to the ENSEMBLE system at EC-JRC, at specified monitoring stations in EU
242 and NA, as well as surface gridded data (Galmarini et al, 2012; Im et al., 2015a, b; Solazzo et
243 al., 2017b). This study investigates the impacts of emission perturbations and boundary
244 conditions on O₃, NO₂, CO, SO₂, PM₁₀ and PM_{2.5} levels over Europe and North America.

245 Differences between each perturbation scenario and the base case (C-IFS global and regional
246 models run with baseline emissions) are calculated from the gridded hourly pollutant fields,
247 which are then monthly and annually averaged in order to estimate the impact of the
248 perturbation of the corresponding emission or boundary condition.

249 To estimate the contribution of foreign emission perturbations relative to the GLO
250 perturbation, we have also calculated the RERER metric (Galmarini et al., 2017; Huang et al.,
251 2017; Jason et al., 2017). For Europe, RERER is calculated using the differences between the
252 GLO vs BASE as well as the differences between EUR vs. BASE simulations for Europe
253 (Eq. 1) while for North America; RERER is calculated using the differences between the
254 GLO vs BASE and NAM vs. BASE simulations (Eq. 2).

255
$$RERER_{EUR} = \frac{R_{GLO} - R_{EUR}}{R_{GLO}} \quad \text{Eq. 1}$$

256
$$RERER_{NAM} = \frac{R_{GLO} - R_{NAM}}{R_{GLO}} \quad \text{Eq. 2}$$

257 where R_{GLO} is the response of the concentration of a given species to global emission
 258 reduction, R_{EUR} is the response of a concentration of a species to the EUR perturbation for the
 259 European domain, and R_{NAM} is the response of a concentration of a specie to the NAM
 260 perturbation for the North American domain. Therefore, a subset of modelling groups that
 261 have conducted the three simulations (BASE, GLO and EUR/NAM for Europe and North
 262 America, respectively) have been used in the metric calculations (see Table 1). The higher the
 263 local response is, the smaller the RERER metric is. The RERER value can exceed the value 1
 264 when emission reductions lead to increasing concentrations (e.g., O₃ titration by nitrogen
 265 monoxide, NO).

266 3. Results

267 3.1. Model Evaluation

268 The base case simulation of each model has been evaluated on a monthly-mean basis using
 269 available surface observations from Europe and North America. The observational data used
 270 in this study are the same as the dataset used in the second phase of AQMEII (Im et al.,
 271 2015a,b). The data were provided from the surface air quality monitoring stations operating
 272 in EU and NA. In EU, surface data were provided by the European Monitoring and
 273 Evaluation Programme (EMEP, 2003; <http://www.emep.int/>) and the European Air Quality
 274 Database (AirBase; <http://acm.eionet.europa.eu/databases/airbase/>). NA observational data
 275 were obtained from the NATChem (Canadian National Atmospheric Chemistry) database and
 276 from the Analysis Facility operated by Environment Canada (<http://www.ec.gc.ca/natchem/>).

Field Code Changed

Field Code Changed

277 The model evaluation results for each model are presented in Fig. 1 and 2, and in Table 3,
 278 along with the results for the multi model (MM) mean and median values. The results show
 279 that the monthly variations of gaseous pollutants are well captured by all models with
 280 correlation coefficients (r) generally higher than 0.70. The biases in simulated O₃ levels are
 281 generally less than 10% with a few exceptions of up to -35%. The temporal variations of NO₂
 282 levels are also well simulated ($r > 0.7$), but exhibit much higher biases, with underestimations
 283 up to 75%. CO levels are underestimated by up to 45% while a majority of the models
 284 underestimated SO₂ levels by up to 68%. Few models overestimated SO₂ by up to 49%. PM₁₀
 285 and PM_{2.5} levels are underestimated by 20% to 70%. Slightly higher biases are calculated for
 286 the PM₁₀ levels.

287 The model biases can be attributed to meteorology, in particular wind speed and planetary
 288 boundary layer (PBL) height, as well as the aerosol mechanisms used in different models that
 289 can underestimate either the inorganic aerosols (e.g. IT2) or the secondary organic aerosols
 290 (e.g. DK1), leading to underestimations in simulated PM mass. As discussed in Solazzo et al.
 291 (2017), EU3 region that covers the central Europe including the Alps has the largest errors in
 292 terms of wind speed, mainly attributed to the diurnal component of the error, with some

293 models having also large errors in the synoptic component. This region also represents the
294 lowest correlation coefficients for all models. They further conclude that emissions and their
295 vertical distribution are the main source of model biases; in particular for the primary species
296 such as CO and PM. Regarding O₃, they found that the models have highest biases in the
297 large scale synoptic component while the diurnal variations are well-captured in general. A
298 more comprehensive evaluation of the models is presented in Solazzo et al. (2017b),
299 Galmarini et al. (2017) and Im et al. (2018⁷).

300 C-IFS base case results have also been evaluated along with the regional CTMs, as presented
301 in Fig. 1 and 2 and in Table 3. The seasonal variations for O₃, NO₂, CO and SO₂ are well
302 captured with high correlation values of ~0.9. PM₁₀ and PM_{2.5} showed a different seasonal
303 cycle than the observation by not reproducing the wintertime maxima ($r \sim -0.7$). C-IFS model
304 underestimates O₃ and CO by ~20% over Europe while NO₂ is slightly overestimated
305 ($NMB=7\%$). SO₂ is overestimated by ~10% over Europe, while PM₁₀ and PM_{2.5} levels are
306 largely underestimated by ~60%, which can be attributed to the lack of secondary aerosol
307 mechanism in the bulk C-IFS model. Over the North American domain, C-IFS well captures
308 the seasonal variations of O₃, NO₂ and CO with correlation coefficients larger than 0.7, while
309 the seasonal variation of SO₂ is not captured by the model ($r=0.04$). The seasonal variations
310 of PM₁₀ and PM_{2.5} are also poorly captured ($r<0.2$). North American O₃ levels are slightly
311 underestimated ($NMB=-10\%$), while NO₂ and CO are overestimated by ~40% and 20%,
312 respectively. SO₂ is overestimated by 35% ~~5~~ while PM₁₀ is largely underestimated by ~80
313 and PM_{2.5} by ~40%. Over both Europe and North America, the wintertime PM levels are
314 underestimated due to lack of secondary aerosols while the spring summer peaks are
315 attributed to long range transport of desert dust from the Sahara, which effect-affects mainly
316 the South East of North America.

317 3.2. Perturbation Analyses

318 The annual mean relative differences of each perturbation scenario from the base case
319 scenario, averaged over all stations, are provided in Table 4 (EU) and Table 5 (NA) for each
320 modeling group, along with the results for the MM ensemble mean and median. The base
321 case monthly mean time series for the participating groups are provided in Fig.1 and Fig. 2
322 for each pollutant, while Fig.3 and Fig. 4 shows the annual mean spatial distribution of the
323 pollutants from the MM ensemble mean calculations over Europe and North America,
324 respectively. As seen in the time series figures, there is a large spread among different
325 groups, owing to the different models used and the different sets of anthropogenic emissions
326 (Table 1). However, the temporal variation is consistent among all models, in particular for
327 the gaseous species.

328 3.2.1. Impact of the global emission reduction scenario (GLO)

329 3.2.1.1. Europe

330 The monthly time series of the differences between the GLO and the BASE simulations for
331 each pollutant are presented in Fig. 5. The annual differences are reported in Table 4.
332 Regarding the primary gaseous pollutants, all models simulate the smallest differences during

333 the summer months while the differences are largest in winter. For O₃, the simulated
334 differences are positive in winter and negative in summer for all models except for DE1 that
335 simulated a decrease in all months. Results suggest that wintertime O₃ over Europe is mainly
336 controlled by anthropogenic emissions. For the other pollutants, results suggest that their
337 levels are mainly controlled by anthropogenic emission throughout the year. The annual
338 difference is smallest for O₃, with a reduction of -0.34 ± 1.23 ppb ($-1.04 \pm 4.00\%$). The annual
339 mean value of the O₃ daily maximum of 8-hour running average decreases by -0.53 ± 1.50 ppb
340 ($-1.62 \pm 3.99\%$). NO₂ levels decreased by 0.97 ± 0.45 ppb ($19.34 \pm 1.59\%$) over Europe while
341 CO levels decreased by 17.35 ± 4.03 ppb ($11.22 \pm 1.17\%$), SO₂ levels by 0.18 ± 0.05 ppb
342 ($20.87 \pm 0.93\%$), PM₁₀ by 2.38 ± 0.68 μgm^{-3} ($15.84 \pm 2.12\%$) and PM_{2.5} by 2.02 ± 0.52 μgm^{-3}
343 ($18.30 \pm 1.75\%$). Vivanco et al. (2017) found similar reductions regarding the deposition of
344 sulfur and nitrogen species over Europe. Almost all models simulate an overall decrease of
345 annual mean O₃ levels over EU (-0.94% to -4.65%), with the exception of TR1 that simulated
346 an increase of 9.31%. Regarding other pollutants, all models simulate a decrease during the
347 simulation period. In general, DE1 and TR1 model groups stand out for introducing the
348 smallest and largest differences, particularly for O₃, NO₂, and PM.

349 The geographical distribution of the change in annual mean concentrations in the GLO
350 scenario as simulated by the MM mean is presented in Fig. 6. Regarding O₃, most of Europe
351 is characterized by decreased concentrations (Fig.6a). Over central Europe, where most of the
352 primary emissions are located (e.g. NO_x), O₃ levels slightly increase by ~2%. Emission
353 hotspots, in particular the Benelux area stands out with largest increases (~6%) due to
354 decreased NO_x-titration effect, which can also be seen in Fig. 6b. In addition, O₃ levels over
355 the northern parts of Germany and France, and southern UK are increasing in response to
356 emission reductions. There is also a clear decrease in CO levels (Fig.6c), in particular over
357 central Europe by up to ~16%. All primary species decrease over the whole domain,
358 especially over the industrial hot spots such as in Poland, Po Valley and the Benelux area
359 (Fig.6d). PM levels decrease throughout the domain by up to ~20% (Fig.6e and f).

360 3.2.1.2. North America

361 The seasonal variation of the impact of 20%-decreased global emissions on the North
362 American pollutant levels are presented in Fig.7. All models simulated a small decrease of
363 3% to 5% (Table 5) in O₃ levels with the largest differences in spring to summer (Fig.7a).
364 The mean response to the emission perturbation is estimated to be -1.39 ± 0.27 ppb ($-3.52 \pm$
365 0.80%). The annual mean value of the O₃ daily maximum of 8-hour running average
366 decreases by -1.93 ± 0.14 ppb ($-4.51 \pm 0.45\%$). All models simulated a largest NO₂ response in
367 winter. Most models simulated a decrease of NO₂ levels while DK1 estimated an increase
368 (Fig.7b). As shown in Table 5, the models simulated a NO₂ response of $-0.4 - 1.2$ ppb (-17.8
369 $\pm 0.78\%$). Regarding CO, all models simulated very clear seasonal profile of the response to
370 emission reductions, with maximum change in late winter/early spring and the minimum
371 change in summer. Most models simulated a change around -15 to -25 ppb (~11%); with the
372 exception of the DE1 model simulating a decrease of ~9 ppb (~7.9%). The MM mean
373 response is calculated to be 19.2 ± 6.9 ppb ($-11 \pm 2.3\%$). The impact of the emission
374 reduction on SO₂ levels was calculated to be -0.25 ppb to -0.48 ppb ($-20.3 \pm 0.2\%$).

375 The response of PM₁₀ levels to the global emission reduction was calculated to be -2.4 ± 1.8
376 μgm^{-3} ($-32.1 \pm 26.6\%$) (Table 5). The largest relative change was calculated for DE1 (~63%).
377 DK1 has almost a flat response around $-1 \mu\text{gm}^{-3}$, while DE1, which is overlapped with the
378 Median line, and US3 have maximum responses in early spring and mid-autumn, while they
379 simulate a minimum response in winter and late spring. Regarding PM_{2.5}, the multi-model
380 mean response was calculated to be $-1.5 \pm 0.9 \mu\text{gm}^{-3}$ ($-17.2 \pm 1.8\%$). DK1 (overlapped with
381 the Median) and US3 simulated the minimum response in May (Fig.7f), while US3 has a
382 slightly higher second minimum in September. This minimum is also simulated by DE1 as
383 the minimum response. DE1 simulates the lowest response among the three models.

384 The spatial distributions of response of different pollutants to the GLO scenario are presented
385 in Fig.8. O₃ levels are reduced over most of the domain (Fig.8a), with slight increases over
386 the emission hotspots due to reduced effect of NO_x-titration, as seen in Fig.8b, as well as
387 decreased CO levels over the whole domain (Fig.8c). SO₂ levels are also decreased
388 throughout the domain (Fig.8d), with the largest reductions over the Atlantic (attributable to
389 reduction in shipping emissions). The western part of the continent is characterized by the
390 lowest reductions. PM levels are reduced throughout the domain by up to 25% (Fig.8e and f),
391 with the largest reductions over the eastern and central parts of the domain. A large decrease,
392 more pronounced in the PM_{2.5} response, can also be seen over California in the western
393 coastal United States.

394 3.2.2. Impact of the North American emission reduction scenario (NAM)

395 3.2.2.1. Europe

396 NA emission reductions account for a reduction of European O₃ levels of -0.22 ± 0.07 ppb ($-$
397 $0.75 \pm 0.14\%$), with all models simulating a decrease of -0.51% to 0.86% , except for the ES1
398 model that simulated an increase of 1.31% (Table 4). This decrease is in agreement with
399 previous studies, such as the HTAP2 study (UN, 2017) that calculated an O₃ reduction over
400 Europe of 0.22 ppb in response to a 20% decrease in the North American NO_x emissions, and
401 Fiore et al. (2009) that simulated a MM mean response of -0.4 ppb in response to a 20%
402 reduction of anthropogenic emissions in North America. NO₂ levels increase slightly by
403 $0.16 \pm 0.01\%$. The annual mean value of the O₃ daily maximum of 8-hour running average
404 decreases by -0.15 ± 0.27 ppb ($-0.45 \pm 0.77\%$). CO levels also decreased over the EU domain
405 by -1.39 ± 0.27 ppb ($-0.96 \pm 0.22\%$), much higher than ~ 0.1 ppb calculated by Fiore et al.
406 (2009). PM₁₀ and PM_{2.5} levels also decreased slightly by $-0.03 \pm 0.03 \mu\text{gm}^{-3}$ ($-0.21 \pm 0.7\%$) and
407 $-0.02 \pm 0.02 \mu\text{gm}^{-3}$ ($-0.18 \pm 0.25\%$), respectively. The models had different SO₂ responses to
408 the NA emissions. Overall, DE1, ES1 and FRES1 simulated almost no change in the surface
409 SO₂ levels while DK1, ES1 and TR1 simulated an increase (0.10% , 5.75% and 0.01% ,
410 respectively) and FII and UK1 simulated a decrease (-0.02% and -0.03% , respectively).
411 Different responses can be due to different model setups including aqueous chemistry,
412 vertical resolutions and aerosol modules (Solazzo et al., 2017).

413 All models were consistent in simulating the largest impact on O₃ during spring and a second
414 lower peak in autumn (Fig.9a). Surface mean NO₂ concentrations (Fig.9b) increased in most

415 models except for FRES1 that simulated a small decrease except for winter. FII also
416 simulated a decrease during the winter period extending to the transition periods. All models,
417 except for ES1, simulated a similar response of CO concentrations to perturbation to NA
418 emissions, with a distinct seasonality (Fig.9c). The SO₂ response in models is also consistent
419 except for the winter period where there is a large spread in magnitude and the sign of the
420 response (Fig.9d).

421 O₃ levels decreased slightly over the entire European domain by up to 3% (Fig.10a). The
422 largest impact is simulated over the western boundary and gradually decreases eastwards.
423 The response of O₃ levels to NAM emissions is more evident during spring where there is a
424 clear transport from Atlantic to the western/northwestern parts of Europe such as the U.K.,
425 northern France and Scandinavia (Fig. S2a). The transport of Atlantic air masses is also
426 shown for the springtime CO levels over Europe (Fig. S2b). The ensemble mean simulates a
427 slight increase of up to 3% in NO₂ levels over Europe (Fig.10b). Along with the O₃ levels,
428 CO levels show the largest decrease over northwestern Europe by up to ~2%. SO₂ levels
429 increased over the whole domain, in particular over Eastern Europe and the Alpine region
430 (Fig.10d), due to a decrease in the oxidative capacity of the atmosphere (see Fig.10a for O₃),
431 leading to a decrease in the SO₂ to SO₄ conversion. This results in an increase of the SO₂
432 levels and a decrease in the PM_{2.5} levels (Fig.10e and f).

433 3.2.2.2. North America

434 The response of North American pollutant levels to a 20% reduction of North American
435 anthropogenic emissions (implemented in both C-IFS and the regional CTMs) are presented
436 in Table 5. The NAM scenario led to a decrease of annual mean O₃ levels over North
437 America by -0.36 ppb (US3) to -0.92 ppb (DE1), with MM ensemble mean calculated to be -
438 0.65 ± 0.28 ppb ($-1.45 \pm 0.88\%$), in agreement with Fiore et al. (2009) that calculated a decrease
439 of ~1 ppb. The annual mean value of the O₃ daily maximum of 8-hour running average
440 decreases by -1.11 ± 0.11 ppb ($-2.60 \pm 0.36\%$), very similar to the change over Europe.
441 Consequently, the largest change in NO₂ levels were simulated by US3 (-1.17 ppb) and
442 smallest by DE1 (-0.36 ppb). The MM mean response of NO₂ is calculated to be -0.71 ± 0.41
443 ppb ($-17.24 \pm 0.58\%$). Similar to NO₂, the largest response in CO levels were simulated by
444 US3 (-19.87 ppb) and the smallest by DE1 (-3.84 ppb), leading to a MM mean response of -
445 12.35 ± 8.06 ppb ($-7.01 \pm 3.60\%$). As seen in Table 5, DE1 simulated a much lower absolute
446 and relative change in CO response compared to DK1 and US3. SO₂ levels decreased by -
447 0.32 ppb to -0.48 ppb, leading to a MM mean response of -0.37 ± 0.09 ppb ($-20 \pm 0.12\%$). PM₁₀
448 levels decreased -1.78 ± 2.08 μgm^{-3} ($-15.78 \pm 3.26\%$). As seen in Table 5, DK1, simulated a
449 very low response to the NAM scenario, by ~ 0.60 μgm^{-3} , compared to the DE1 and the US3
450 groups that simulated a PM₁₀ response of -2.02 μgm^{-3} and -4.19 μgm^{-3} , respectively.
451 However, the relative responses are not very different between the different groups (~16%).

452 The response of O₃ to the NAM scenario is largest in summer (Fig.11a): June for DK1 and
453 US3 and August for DE1. The O₃ response clearly shows a difference from the GLO
454 response in spring, suggesting the impact of long-range transport in spring that does not
455 appear in the perturbation of the local emissions only. The largest NO₂ response (Fig.11b) is

456 simulated by US3, similar to the response to the GLO scenario. The response of CO to the
457 reductions in local emissions (Fig. 11c) is different from the response to the global reduction,
458 where DK1 and US3 has the minimum response in spring and DE1 has the minimum
459 response in autumn. The response of SO₂ and PM to GLO and NAM are similar, suggesting
460 the main drivers of SO₂ and PM levels are local emissions.

461 Annual mean O₃ levels show large reductions (~20%) over the eastern parts of the domain,
462 while there are slight increases or less pronounced decreases over the western parts of the
463 domain (Fig. 12a), associated with larger NO_x reductions (Fig. 12b). CO and SO₂ levels are
464 mostly reduced over the central to eastern parts of the domain (Fig. 12c and d, respectively),
465 with shipping impacts over the Atlantic being more pronounced on SO₂ levels. The western
466 parts of the U.S. experiences smaller SO₂ reductions (~5-10%) and slight increases over the
467 southwestern U.S. The response of PM to the NAM scenario (Fig. 12e and f) is very similar to
468 the response to the GLO scenario (Fig. 8e and f).

469 3.2.3. Impact of the European emission reduction scenario (EUR)

470 O₃ levels increase slightly by 0.01 ± 0.40 ppb ($0.25 \pm 1.35\%$) in response to the 20% reduction
471 of the anthropogenic emissions from Europe (Table 4). This response is much lower than
472 Fiore et al. (2009) that calculated a MM mean response of 0.8 ppb. However, as seen in
473 Fig. 13a, the positive mean response together with the large standard deviation is due to the
474 DE1 model that simulated a decrease (-2.33%), while other groups simulated an increase
475 (0.39% to 1.72%). There is a distinct seasonality in the response with winter levels increasing
476 with reduced emissions and summer levels decreasing, following the emission temporal
477 variability. The annual mean value of the O₃ daily maximum of 8-hour running average
478 decreases by -0.21 ± 0.10 ppb ($-0.62 \pm 0.24\%$). NO₂ concentrations decreased by -0.75 ± 0.26
479 ($17.68 \pm 0.90\%$), with a similar seasonal response of SO₂ levels ($-17.52 \pm 1.70\%$) and CO levels
480 ($-6.26 \pm 1.07\%$), consistent with the findings of Vivanco et al. (2017). An opposite seasonal
481 variation is calculated for the O₃ response (Fig. 13.b-d)., The DE1 model also stands out in
482 the NO₂ response together with the FRES1 model in the magnitude of the response (Fig. 13b).
483 PM₁₀ and PM_{2.5} levels have similar responses to the emissions reduction ($-14.43 \pm 2.84\%$ and -
484 $15.67 \pm 2.12\%$, respectively) with similar seasonality.

485 The MM mean geographical distribution of the O₃ response is very similar with that of the
486 GLO perturbation (Fig. 14a), with relatively smaller decreases by up to ~3%. O₃ levels
487 increase over the central and in particular over northwestern Europe by up to ~6%. NO₂
488 levels decrease uniformly over the entire domain by up to ~20% (Fig. 14b). CO levels
489 decrease over the emission sources, mainly over central and Eastern Europe (Fig. 14c). PM
490 levels also decrease over the entire domain, especially over central and Eastern Europe
491 (Fig. 14e and f).

492 3.2.4. Impact of the East Asian emission reduction scenario (EAS)

493 As seen in Table 5, the impacts of East Asian emissions on North American O₃ levels are
494 much lower than the impacts from the reductions in global and local emissions. The largest
495 impact is simulated by DE1 as -0.99 ppb (-0.35%), while other models give similar responses

496 (~-0.60 ppb; -0.20%). The O₃ response as calculated by the MM mean ensemble is -0.25±0.07
497 ppb, in agreement with the HTAP2 findings and Fiore et al. (2009). The annual mean value
498 of the O₃ daily maximum of 8-hour running average decreases by -0.28±0.07 ppb (-
499 0.65±0.20%). NO₂ and SO₂ response to reductions in EAS emissions were simulated to be
500 very small (-0.04±0.08% and 0.01±0.02%, respectively). The CO response to EAS was
501 simulated to be -2.60 ppb (DE1) to -4.16 ppb (DK1), with the MM mean response of -
502 3.37±0.68 ppb (-2±0.29%). Regarding PM₁₀, DE1 simulated a very large response (~-0.56
503 μgm⁻³) compared to DK1 and US3 (~-0.05 μgm⁻³), leading to a MM mean response of -
504 0.21±0.30 μgm⁻³ (-5.63±8.50%). However, the PM_{2.5} response was much lower (-0.02±0.03
505 μgm⁻³; -0.20±0.35%), suggesting that the PM_{2.5} levels are largely driven by local emissions.

506 The O₃ response to EAS emission reductions was highest in spring and autumn, suggesting
507 that long-range transport is important in these seasons (Fig. 15a). The NO₂ response was
508 negative, being maximum in winter and minimum in summer, except for DK1 showing an
509 increase in NO₂ levels in all seasons (Fig. 15b). The impact of EAS emissions on North
510 American CO levels showed a distinct seasonality (Fig. 15c), similar to the impact of the
511 global emission reductions (Fig. 5c), suggesting that regional CO levels over North America
512 are driven by both local emissions and long-range transport. The response of SO₂ to East
513 Asian emission reductions varied largely from model to model with US3 showing an overall
514 reduction while DE1 and DK1 simulated increases in winter, spring, and autumn, and
515 decreases in summer (Fig. 15d). The PM₁₀ response simulated by DK1 (overlapped with the
516 median) and US3 were simulated to be small, being largest in spring (Fig. 15e). However,
517 DE1 simulated a large and opposite response, with spring having the smallest response and
518 winter with the largest response. DE1 also simulated a different PM_{2.5} response in terms of
519 the sign of the change and thus, seasonality in response to DK1 and US3 (Fig. 15f). Largest
520 differences were simulated in spring, similar to PM₁₀ by DK1 and US3, while DE1 simulated
521 the largest response in winter and summer and the spring response was minimum.

522 The impact of the East Asian emissions over the western parts of North America is clearly
523 seen for all pollutants in Fig. 16. The impacts are low for all pollutants, being up to 5%. The
524 impacts are particularly pronounced for CO (Fig. 16c), SO₂ (Fig. 16d) and PM (Fig. 16e and f).
525 The largest O₃ response was simulated over the northwestern parts of North America
526 (Fig. 16a). The springtime transport of O₃ from East Asia is more evident compared to the
527 annual average of the perturbation response (Fig. S3a), where the western NA O₃ levels
528 decrease by up to ~1.5%. The springtime CO levels also decrease by up to 6% (Fig. S3b),
529 showing the importance of long-range transport from East Asia.

530 3.2.5. RERER analyses

531 As discussed in Section 2, the RERER metric (Galmarini et al., 2017; Hang et al., 2017;
532 Jason et al., 2017) is designed to quantify the relative impact of local vs. non-local emission
533 sources on pollutant levels in the receptor regions EU and NA. ~~Using gridded hourly
534 pollutant concentrations from the base case, GLO and EUR simulations, †~~The RERER
535 metrics for the EU have been calculated using gridded annual mean pollutant concentrations
536 from the BASE, GLO and EUR simulations for the annual mean concentrations response for

537 the individual groups as well as for the ensemble mean. For the NA domain. The RERER
538 metrics have been calculated using the [annual mean concentrations from the base-case BASE](#),
539 GLO and NAM simulations. Table 6 presents the RERER metric calculated for the European
540 domain. The table shows differences in the strengths of non-local source contributions to
541 different species among the different models. Regarding the RERER metric for O₃ in Europe,
542 most values calculated are below one, except for the IT1 model, which shows a significant
543 increase of O₃ levels in Europe in response to emission reductions compared with the other
544 models. A RERER value of 0.8-0.9 is calculated for the majority of models, implying the
545 dominance of non-local sources in Europe, except for the DE1 model, where the RERER
546 value is lower (~0.5), giving an equal contribution of local vs. non-local sources in Europe.
547 The MM mean RERER value for O₃ is ~0.8, showing a much larger contribution of non-local
548 sources compared to local sources in Europe. This result is in agreement with, however
549 slightly smaller, Jonson et al. (2017) that calculated a MM mean RERER value of 0.89.

550 Regarding NO₂, the RERER metrics (< 0.4) show that NO₂ is controlled by local sources. In
551 addition, the RERER metrics calculated for DE1 and FI1 are slightly negative, implying that
552 the signal is not sensitive to non-local emissions. RERER calculated for the ensemble mean
553 for NO₂ (~0.2) also shows the high sensitivity of NO₂ concentrations to local sources. The
554 RERER metric calculations for CO shows similar contributions from local vs. non-local
555 sources, with RERER values of 0.4-0.6, except for IT1. IT1 has a RERER metric value of
556 ~0.9 suggesting a large contribution of non-local sources, leading to the higher sensitivity of
557 CO to non-local sources compared to other model groups. The RERER values calculated for
558 the ensemble mean (~0.6) shows a slightly larger contribution of non-local sources compared
559 to local sources. The MM mean RERER value of 0.55 for CO from this study is in very good
560 agreement with Jonson et al. (2017) that calculated a MM mean RERER of 0.51. RERER
561 metrics calculated for SO₂ are also in the low range (0-0.4). While DE1 and FI1 show almost
562 no signal for the non-local contribution, DK1, IT1 and UK1 are in the higher end of the
563 range. The CO MM mean RERER value of ~0.3 shows that CO levels are largely controlled
564 by local emissions. Finally, the metrics calculated for PM₁₀ and PM_{2.5} shows that local
565 sources are the main contributor to the PM levels in Europe (RERER = ~0 - 0.3), leading to
566 an ensemble mean contribution of local sources (RERER = ~0.2).

567

568 Regarding the local vs. non-local contributions to different pollutants over the North
569 American domain, three groups out of four simulated the GLO and NAM scenarios needed to
570 calculate the RERER metrics. RERER metrics show that O₃ is largely controlled by non-local
571 sources. European model groups DE1 and DK1 simulate a larger influence of non-local
572 sources (~0.8 - ~0.9) compared to the US3 group, which simulated lower RERER metric
573 values of ~0.5, indicating that O₃ levels are driven equally by local and non-local sources.
574 This lower value is also consistent with the findings of Huang et al. (2017), who simulated
575 the largest impacts on O₃ in May and June with RERER values around ~0.5. The ensemble
576 mean shows that O₃ responses are largely attributable to non-local sources (RERER = ~0.8),
577 which are similar to those found for Europe. RERER metric values calculated for NO₂ by
578 different models (RERER = ~0 - ~0.2) and the ensemble mean (RERER = 0.05) clearly

579 shows that NO₂ is controlled by local sources, similar to the Europe case. The sensitivity of
580 CO to local and non-local sources are similar to those for O₃, with DE1 and DK1 simulating a
581 large contribution from non-local sources while US1 shows that CO is controlled equally by
582 local and non-local sources (RERER = 0.5). Similar to NO₂, all models show that SO₂ is
583 largely driven by local sources with RERER values between ~0.1 and ~0.2. Regarding the
584 particles, models simulate very similar responses to changes in the local and non-local
585 sources. RERER values are calculated to be ~0.08 and ~0.11 for PM₁₀ and PM_{2.5},
586 respectively, showing the large local contribution compared to non-local sources.

587 Fig. 17 shows the spatial distributions of the MMM RERER values for O₃ and PM_{2.5}, as
588 constructed from the annual mean responses to perturbation scenarios over Europe and North
589 America. Fig. 17a shows that O₃ is dominantly controlled by non-local sources with RERER
590 values higher than 0.5 throughout the domain. Higher values are calculated over the north
591 western Europe, in particular over UK and the north western part of the domain covering the
592 Atlantic. In contrary, PM_{2.5} levels are controlled by local sources with RERER values around
593 0.2 (Fig. 17b). North American O₃ levels are largely controlled by non-local sources over the
594 western part of the domain, with RERER values above 0.5 (Fig. 17c). Local sources play a
595 more important role in controlling O₃ levels over the eastern part of the U.S. where much
596 lower RERER values are calculated. PM_{2.5} levels are dominantly controlled by the local
597 sources, similar to the case in Europe, with low RERER values throughout the domain (Fig.
598 17d). PM_{2.5} levels over the western part of the domain has however a relatively larger
599 contribution from non-local sources. It is important to note that the sharp gradients in the
600 PM_{2.5} RERER values over both the eastern part of the Europe domain and the Mexican part
601 of the NA domain is due to HTAP2-definition of source regions where the perturbations are
602 introduced. Therefore, due to the large contribution of the local sources to PM_{2.5} levels, large
603 gradients are calculated across the HTAP2 borders. As O₃ is largely controlled by non-local
604 sources, these gradients do not exist.

605 In order to further analyze the impact of local vs non-local sources, the monthly variations of
606 RERER values for O₃ and PM_{2.5} over both domains are presented in Fig. 18. All models
607 simulate a larger non-local source contribution during the spring period for both domains and
608 pollutants. For both pollutants and domains, the local sources have relatively larger
609 contribution in winter periods, reflected by the lower RERER values compared to other parts
610 of the year. Regarding European O₃, majority of the models show a RERER value of between
611 0.5 and 1, while DE1 shows much lower and IT1 much higher values (see also Table 6). DE1
612 and FI1 simulates the lowest RERER values for PM_{2.5} (< 0.1), while other models calculate
613 RERER values between 0.1 and 0.5. Regarding O₃ over North America, US3 shows that in
614 winter months, O₃ is controlled more by local emission with RERER values much lower than
615 0.5, while DE1 shows the highest non-local contributions throughout the year.

616

617 **CONCLUSIONS**

618 In the framework of the third phase of the Air Quality Model Evaluation International
619 Initiative (AQMEII3), the impacts of local vs. foreign emissions over the European and North
620 American receptor regions are simulated by introducing a 20% decrease of global and
621 regional emissions by research groups, using different state-of-the-art chemistry and transport
622 models. The emission perturbations were introduced globally, as well as over the HTAP2-
623 defined regions of Europe, North America and East Asia. Base case and the perturbation
624 scenarios are first simulated using the global C-IFS global model, which provides the
625 boundary conditions to the regional CTMs.

626 The base case simulation of each model has been evaluated against surface observations from
627 Europe and North America. The temporal variabilities of all pollutants are well captured by
628 all models with correlations generally higher than 0.70. O₃ levels are generally simulated
629 with a *MNB* less than 10% with few exceptions of *MNB* values up to -35%. NO₂, CO and
630 SO₂ levels are simulated with underestimations up to 75%, 45% and 68%, respectively. PM₁₀
631 and PM_{2.5} levels are underestimated by 20% to 70%, with slightly higher biases in PM₁₀
632 levels.

633 Results from the perturbation simulations show that the largest impacts over both Europe and
634 North American domains are simulated in response to the global emission perturbation
635 (GLO). These responses are similar, however slightly lower, as compared to the local
636 emission perturbation scenarios for Europe (EUR) and North America (NAM). In contrast to
637 the GLO scenario, O₃ levels over Europe slightly increase by 0.13 ppb (0.02%). The annual
638 mean value of the O₃ daily maximum of 8-hour running average decreases in all scenarios
639 over Europe, highest in the GLO scenario by ~1% and lowest in the NAM scenario by
640 ~0.3%. Over North America, the annual mean value of the O₃ daily maximum of 8-hour
641 running average decreased by ~5% in the GLO scenario, 3% in the NAM scenario and 0.7%
642 in the EAS scenario. The impact of foreign emissions simulated by the NAM scenario for
643 Europe and EAS scenario for North America were found to be lowest, however still
644 noticeable, particularly close to the boundaries. This impact is especially noticeable (up to
645 only a few percent) for the western parts of the North American domain in response to the
646 emission reductions over East Asia. The response is almost linear (~20% decrease) to the
647 change in emissions for NO₂, SO₂ and PM in the global perturbation scenario (GLO), while
648 O₃ levels decrease slightly (~1%).

649 Despite these small differences, there are large geographical differences. NO₂, CO and SO₂
650 levels are mainly affected over emission hot spots in the GLO scenario as well as in the EUR
651 scenario for Europe and the NAM scenario for North America. O₃ levels increase over the hot
652 spot regions, in particular the Benelux region in Europe, by up to ~6% due to the reduced
653 effect of NO_x-titration. Over the North American domain, the central-to-eastern part and the
654 western coast of the U.S experience the largest response to the global emission perturbation.
655 For most of the pollutants, there is distinct seasonality in the responses particularly to the
656 global and local emission perturbations. The largest responses are calculated during winter
657 months, where anthropogenic emission are highest, except for O₃, where largest responses are
658 seen during spring/summer months, suggesting photochemistry still plays an important role in
659 O₃ levels.

660 The RERER metrics have been calculated to examine the differences in the strengths of non-
661 local source contributions to different species among the different models. The large RERER
662 values over Europe and North America for O₃ (~0.8), show a larger contribution of non-local
663 sources, while for other gaseous pollutants (NO₂, CO and SO₂) and particles (PM₁₀ and
664 PM_{2.5}), low RERER values (< 0.5) indicate that these pollutants are largely controlled by
665 local sources. Results show that the contribution of local sources on NO₂, SO₂ and PM levels
666 are larger in North America compared to Europe, while for CO, local sources have a larger
667 share in Europe in comparison with North America. In addition, RERER analyses shows that
668 European O₃ is largely controlled by non-local sources (RERER > 0.5) throughout the
669 domain. PM_{2.5} levels are largely controlled by local sources with RERER values around 0.2
670 throughout the domain. Local sources play a more important role in controlling O₃ levels
671 over the eastern part of the U.S. PM_{2.5} levels over the western part of NA has a relatively
672 larger contribution from non-local sources compared to the rest of the domain. A larger non-
673 local source contribution during the spring period for both domains and pollutants has been
674 calculated, suggesting long-range transport from non-local sources. For both pollutants and
675 domains, the local sources have relatively larger contribution in winter periods, reflected by
676 the lower RERER values compared to other parts of the year.

677 Overall results show that there is a large spread among the models, although the majority of
678 the models simulate a similar seasonal variation. These differences suggest that despite the
679 harmonization of inputs, such as emissions and boundary conditions, to regional models,
680 there are still large differences between models, such as different gas phase and aerosol
681 modules, deposition schemes, meteorological drivers and spatial and vertical resolutions.
682 Therefore, the use of multi model ensembles can help to reduce the uncertainties inherent in
683 individual models.

684

685 ACKNOWLEDGEMENTS

686 We gratefully acknowledge the contribution of various groups to the third air Quality Model
687 Evaluation international Initiative (AQMEII) activity. Joint Research Center Ispra/Institute
688 for Environment and Sustainability provided its ENSEMBLE system for model output
689 harmonization and analyses and evaluation. The views expressed in this article are those of
690 the authors and do not necessarily represent the views or policies of the U.S. Environmental
691 Protection Agency. Aarhus University gratefully acknowledges the NordicWelfAir project
692 funded by the NordForsk's Nordic Programme on Health and Welfare (grant agreement no.
693 75007), the REEEM project funded by the H2020-LCE Research and Innovation Action
694 (grant agreement no.: 691739), and the Danish Centre for Environment and Energy (AU-
695 DCE). University of L'Aquila thanks the EuroMediterranean Center for Climate Research
696 (CMCC) for providing the computational resources. RSE contribution to this work has been
697 financed by the research fund for the Italian Electrical System under the contract agreement
698 between RSE S.p.A. and the Ministry of Economic Development – General Directorate for
699 Nuclear Energy, Renewable Energy and Energy Efficiency in compliance with the decree of
700 8 March 2006. CIEMAT has been financed by the Spanish Ministry of Agriculture and Food,

701 Fishing and Environment. University of Murcia thanks the Spanish Ministry of Economy for
702 the research contract CGL2014-59677-R (also partially funded by the FEDER programme).

703

704 REFERENCES

705 Akimoto, H. (2003), Global air quality and pollution, *Science*, 302, 1716–1719,
706 doi:10.1126/science.1092666.

707 Andersson, E., Kahnert, M., and Devasthale, A.: Methodology for evaluating lateral
708 boundary conditions in the regional chemical transport model MATCH (v5.5.0) using
709 combined satellite and ground-based observations, *Geosci. Model Dev.*, 8, 3747-3763,
710 <https://doi.org/10.5194/gmd-8-3747-2015>, 2015.

711 Fiore, A., Dentener, F., Wild, O., Cuvelier, C., Schultz, M., Textor, C., Schulz, M., Atherton,
712 C., Bergmann, D., Bey, I., Carmichael, G., Doherty, R., Duncan, B., Faluvegi, G., Folberth,
713 G., Garcia Vivanco, M., Gauss, M., Gong, S., Hauglustaine, D., Hess, P., Holloway, T.,
714 Horowitz, L., Isaksen, I., Jacob, D., Jonson, J., Kaminski, J., Keating, T., Lupu,
715 A., MacKenzie, I., Marmer, E., Montanaro, V., Park, R., Pringle, K., Pyle, J., Sanderson, M.,
716 Schroeder, S., Shindell, D., Stevenson, D., Szopa, S., Van Dingenen, R., Wind, P., Wojcik,
717 G., Wu, S., Zeng, G., and Zuber, A.: Multi-model estimates of intercontinental source-
718 receptor relationships for ozone pollution, *J. Geophys. Res.*, 114,
719 doi:10.1029/2008JD010816, 2009.

720 Flemming, J., Huijnen, V., Arteta, J., Bechtold, P., Beljaars, A., Blechschmidt, A.-M.,
721 Diamantakis, M., Engelen, R. J., Gaudel, A., Inness, A., Jones, L., Josse, B., Katragkou, E.,
722 Marecal, V., Peuch, V.-H., Richter, A., Schultz, M. G., Stein, O., and Tsikerdekis, A., 2015.
723 Tropospheric chemistry in the Integrated Forecasting System of ECMWF, *Geosci. Model*
724 *Dev.*, 8, 975-1003, doi:10.5194/gmd-8-975-2015

725

726 Galmarini, S., Koffi, B., Solazzo, E., Keating, T., Hogrefe, C., Schulz, M., Benedictow, A.,
727 Griesfeller, J. J., Janssens-Maenhout, G., Carmichael, G., Fu, J., and Dentener, F.: Technical
728 note: Coordination and harmonization of the multi-scale, multi-model activities HTAP2,
729 AQMEII3, and MICS-Asia3: simulations, emission inventories, boundary conditions, and
730 model output formats, *Atmos. Chem. Phys.*, 17, 1543-1555, [https://doi.org/10.5194/acp-17-](https://doi.org/10.5194/acp-17-1543-2017)
731 [1543-2017](https://doi.org/10.5194/acp-17-1543-2017), 2017.

732 Galmarini S, Bianconi R, Appel W, Solazzo E, Mosca S, Grossi P, et al (2012) ENSEMBLE
733 and AMET: Two systems and approaches to a harmonized, simplified and efficient facility
734 for air quality models development and evaluation. *Atmos Environ* 53: 51-59.

735 Galmarini, S., Kioutsioukis, I., and Solazzo, E.: E pluribus unum*: ensemble air quality
736 predictions, *Atmos. Chem. Phys.*, 13, 7153-7182, <https://doi.org/10.5194/acp-13-7153-2013>,
737 2013.

738 Giordano, L., Brunner, D., Flemming, J., Hogrefe, C., Im, U., Bianconi, R., Badia, A.,
739 Balzarini, A., Baro, R., Chemel, C., Curci, G., Forkel, R., Jimenez-Guerrero, P., Hirtl, M.,
740 Hodzic, A., Honzak, L., Jorba, O., Knote, C., Kuenen, J.J.P., Makar, P.A., Manders-Groot,
741 A., Neal, L., Perez, J.L., Pirovano, G., Pouliot, G., San Jose, R., Savage, N., Schroder, W.,
742 Sokhi, R.S., Syrakov, D., Torian, A., Tuccella, P., Werhahn, J., Wolke, R., Yahya, K.,
743 Žabkar, R., Zhang, Y., Galmarini, S., 2015. Assessment of the MACC reanalysis and its
744 influence as chemical boundary conditions for regional air quality modeling in AQMEII-2.
745 *Atmospheric Environment*, 115, 371-388.

746 Hogrefe, C., Liu, P., Pouliot, G., Mathur, R., Roselle, S., Flemming, J., Lin, M., and Park, R.
747 J.: Impacts of Different Characterizations of Large-Scale Background on Simulated
748 Regional-Scale Ozone Over the Continental United States, *Atmos. Chem. Phys. Discuss.*,
749 <https://doi.org/10.5194/acp-2017-676>, in review, 2017

750 Holloway, T., Fiore, A., Hastings, M.G., 2003, Intercontinental transport of air pollution:
751 Will emerging science lead to a new hemispheric treaty?, *Environ. Sci. Technol.*, 37, 4535 –
752 4542, doi:10.1021/es034031g.

753 Huang, M., Carmichael, G. R., Pierce, R. B., Jo, D. S., Park, R. J., Flemming, J., Emmons, L.
754 K., Bowman, K. W., Henze, D. K., Davila, Y., Sudo, K., Jonson, J. E., Tronstad Lund, M.,
755 Janssens-Maenhout, G., Dentener, F. J., Keating, T. J., Oetjen, H., and Payne, V. H.: Impact
756 of intercontinental pollution transport on North American ozone air pollution: an HTAP
757 phase 2 multi-model study, *Atmos. Chem. Phys.*, 17, 5721-5750, <https://doi.org/10.5194/acp-17-5721-2017>, 2017.

759 Husar, R.B., Tratt, D.M., Schichtel, D.M., Falke, S.R., Li, F., Jaffe, D., Gassó, S., Gill, T.,
760 Laulainen, N. S., Lu, F., Reheis, M.C., Chun, Y., Westphal, D., Holben, B.N., Gueymard, C.,
761 McKendry, I., Kuring, N., Feldman, G.C., McClain, C., Frouin, R.J., Merrill, J., DuBois, D.,
762 Vignola, F., Murayama, T., Nickovic, S., Wilson, W. E., Sassen, K., Sugimoto, N., Malm,
763 W.C., 2001. Asian dust events of April 1998. *J. Geophys. Res.*, 106 (D16), 18317 – 18330,
764 doi:10.1029/2000JD900788.

765 Huszar, P., Belda, M., and Halenka, T.: On the long-term impact of emissions from central
766 European cities on regional air quality, *Atmos. Chem. Phys.*, 16, 1331-1352,
767 <https://doi.org/10.5194/acp-16-1331-2016>, 2016.

768 Im, U., Brandt, J., Geels, C., Hansen, K.M., Christensen, J.H., Andersen, M.S., Solazzo, E.,
769 Kioutsioukis, I., Alyuz, U., Balzarini, A., Baro, R., Bellasio, R., Bianconi, R., Bieser, J.,
770 Colette, A., Curci, G., Farrow, A., Flemming, J., Fraser, A., Jimenez-Guerrero, P., Kai-Chai,
771 L., Kitwiroon, N., Pirovano, G., Pozzoli, L., Prank, M., Rose, R., Sokhi, R., Tuccella, P.,
772 Unal, A., Vivanco, M.G., West, J., Yardwood, G., Hogrefe, C., Galmarini, S., 2017. Air
773 pollution impacts on human health and the associated external costs over Europe and the
774 United States as calculated by a multi-model ensemble in frame of AQMEII3, *Atmospheric
775 Chemistry and Physics*, Under Review.

776 Im, U., Bianconi, R., Solazzo, E., Kioutsioukis, I., Badia, A., Balzarini, A., Baro, R.,
777 Bellasio, R., Brunner, D., Chemel, C., Curci, G., Denier van der Gon, H.A.C., Flemming, J.,
778 Forkel, R., Giordano, L., Jimenez-Guerrero, P., Hirtl, M., Hodzic, A., Honzak, L., Jorba, O.,
779 Knote, C., Makar, P.A., Manders-Groot, A., Neal, L., Perez, J.L., Pirovano, G., Pouliot, G.,
780 San Jose, R., Savage, N., Schroder, W., Sokhi, R.S., Syrakov, D., Torian, A., Tuccella, P.,
781 Werhahn, K., Wolke, R., Yahya, K., Zabkar, R., Zhang, Y., Zhang, J., Hogrefe, C.,
782 Galmarini, S., 2015b. Evaluation of operational online-coupled regional air quality models
783 over Europe and North America in the context of AQMEII phase 2. Part II: Particulate
784 Matter. *Atmospheric Environment*, 115, 421-441.

785 Im, U., Bianconi, R., Solazzo, E., Kioutsioukis, I., Badia, A., Balzarini, A., Baro, R.,
786 Bellasio, R., Brunner, D., Chemel, C., Curci, G., Flemming, J., Forkel, R., Giordano, L.,
787 Jimenez-Guerrero, P., Hirtl, M., Hodzic, A., Honzak, L., Jorba, O., Knote, C., Kuenen, J.J.P.,
788 Makar, P.A., Manders-Groot, A., Neal, L., Perez, J.L., Piravano, G., Pouliot, G., San Jose, R.,
789 Savage, N., Schroder, W., Sokhi, R.S., Syrakov, D., Torian, A., Werhahn, K., Wolke, R.,
790 Yahya, K., Zabkar, R., Zhang, Y., Zhang, J., Hogrefe, C., Galmarini, S., 2015a. Evaluation of
791 operational online-coupled regional air quality models over Europe and North America in the
792 context of AQMEII phase 2. Part I: Ozone. *Atmospheric Environment*, 115, 404-420.

793 Im, U. and Kanakidou, M.: Impacts of East Mediterranean megacity emissions on air quality,
794 *Atmos. Chem. Phys.*, 12, 6335-6355, <https://doi.org/10.5194/acp-12-6335-2012>, 2012.

795 Jaffe, D., Bertschi, I., Jaegle, L., Novelli, P., Reid, J.S., Tanimoto, H., Vingarzan, R.,
796 Westphal, D.L., 2004. Long-range transport of Siberian biomass burning emissions and
797 impact on surface ozone in western North America. *Geophys. Res. Lett.*, 31, L16106,
798 doi:10.1029/2004GL020093.

799 Janssens-Maenhout, G., Crippa, M., Guizzardi, D., Dentener, F., Muntean, M., Pouliot, G.,
800 Keating, T., Zhang, Q., Kurokawa, J., Wankmüller, R., Denier van der Gon, H., Kuenen, J. J.
801 P., Klimont, Z., Frost, G., Darras, S., Koffi, B., and Li, M.: HTAP_v2.2: a mosaic of regional
802 and global emission grid maps for 2008 and 2010 to study hemispheric transport of air
803 pollution, *Atmos. Chem. Phys.*, 15, 11411–11432, doi:10.5194/acp-15-11411-2015, 2015.

804 Jiménez, P., Parra, R., and Baldasano, J. M.: Influence of initial and boundary conditions for
805 ozone modeling in very complex terrains: a case study in the northeastern Iberian Peninsula,
806 *Environ. Modell. Softw.*, 22, 1294–1306, 2007.

807 Jonson, J.E., Schulz, M., Emmons, L., Flemming, J., Henze, D., Sudo, K., Lund, M.T., Lin,
808 M., Benedictow, A., Koffi, B., Eckhart, P., Dentener, F., Keating, T., 2017. The effects of
809 intercontinental emission sources on European air pollution levels. In preparation for *Atmos.*
810 *Chem. Phys.*

811 Kioutsioukis, I., Im, U., Solazzo, E., Bianconi, R., Badia, A., Balzarini, A., Baró, R.,
812 Bellasio, R., Brunner, D., Chemel, C., Curci, G., Denier van der Gon, H., Flemming, J.,
813 Forkel, R., Giordano, L., Jiménez-Guerrero, P., Hirtl, M., Jorba, O., Manders-Groot, A.,
814 Neal, L., Pérez, J. L., Pirovano, G., San Jose, R., Savage, N., Schroder, W., Sokhi, R. S.,

815 Syrakov, D., Tuccella, P., Werhahn, J., Wolke, R., Hogrefe, C., and Galmarini, S.: Improving
816 the deterministic skill of air quality ensembles, *Atmos. Chem. Phys.*, 16, 15629-15652.

817 Li, Q., Jacob, D.J., Bey, I., Palmer, P.I., Duncan, B.N., Field, B.D., Martin, R.V., Fiore,
818 A.M., Yantosca, R.M., Parrish, D.D., Simmonds, P.G., Oltmans, S.J., 2002. Transatlantic
819 transport of pollution and its effects on surface ozone in Europe and North America. *J.*
820 *Geophys. Res.*, 107, D13, 4166, 10.1029/2001JD001422.

821 Liang, C., Silva, R.A., West, J.J., Emmons, L., Jonson, J.E., Bian, H., Pan, X., Chin, M.,
822 Henze, D., Lund, M.T., Sudo, K., Sekiya, T., Takemura, T., Flemming, J., Park, R., Lin, M.,
823 Pierce, R.B., Lenzen, A., Kucsera, T., Folberth, G., 2017. Multi-model estimates of
824 premature human mortality due to intercontinental transport of air pollution. *Atmospheric*
825 *Chemistry and Physics*, In preparation for *Atmos. Chem. Phys.*

826 Mason, R., Zubrow, A., Eyth, A., 2007. Technical Support Document (TSD) Preparation of
827 Emissions Inventories for the Version 5.0, 2007 Emissions Modeling Platform, available at:
828 <https://www.epa.gov/air-emissions-modeling/2007-version-50-technical-support-document>,
829 last access: 24 May 2017.

830 Mathur, R.: Estimating the impact of the 2004 Alaskan forest fires on episodic particulate
831 matter pollution over the eastern United States through assimilation of satellite-derived
832 aerosol optical depths in a regional air quality model, *J. Geophys. Res.*, 113, D17302,
833 doi:10.1029/2007JD009767, 2008.

834 Pouliot, G., Denier van der Gon, H., Kuenen, J., Makar, P., Zhang, J., Moran, M., 2015.
835 Analysis of the emission inventories and model-ready emission datasets of Europe and North
836 America for phase 2 of the AQMEII project. *Atmos. Environ.* 115, 345-360.

837 Rao, S., Mathur, R., Hogrefe, C. Keating, T., Dentener, F., and Galmarini, S.: Path Forward
838 for the Air Quality Model Evaluation International Initiative (AQMEII), *EM, Air And Waste*
839 *Management Associations Magazine For Environmental Managers*, 7, 38–41, 2012.

840 Rudich, Y., Kaufman, Y. J., Dayan, U., Yu, H., and Kleidman, R. G.: Estimation of
841 transboundary transport of pollution aerosols by remote sensing in the eastern Mediterranean,
842 *J. Geophys. Res.*, 113, D14S13, doi:10.1029/2007JD009601, 2008.

843 Solazzo, E., Bianconi, R., Hogrefe, C., Curci, G., Alyuz, U., Balzarini, A., Baró, R., Bellasio,
844 R., Bieser, J., Brandt, J., Christensen, J. H., Colette, A., Francis, X., Fraser, A., Garcia
845 Vivanco, M., Jiménez-Guerrero, P., Im, U., Manders, A., Nopmongcol, U., Kitwiroon, N.,
846 Pirovano, G., Pozzoli, L., Prank, M., Sokhi, R. S., Tuccella, P., Unal, A., Yarwood, G., and
847 Galmarini, S., 2017b. Evaluation and Error Apportionment of an Ensemble of Atmospheric
848 Chemistry Transport Modelling Systems: Multi-variable Temporal and Spatial Breakdown,
849 *Atmos. Chem. Phys.*, 17, 3001-3054.

850 Solazzo, E., Hogrefe, C., Colette, A., Garcia-Vivanco, M., Galmarini, S., 2017a. Advanced
851 error diagnostics of the CMAQ and Chimere modelling systems within the AQMEII3 model

852 evaluation framework. *Atmos. Chem. Phys.*, 17, 10435-10465, <https://doi.org/10.5194/acp->
853 17-10435-2017.

854 Solazzo, E., Riccio, A., Kioutsioukis, I., Galmarini, S., 2013b. Pauci ex tanto numero: reduce
855 redundancy in multi-model ensembles. *Atmos. Chem. Phys.* 13, 8315-8333.

856 Solazzo, E., Bianconi, R., Vautard, R., Appel, K.W., Moran, M.D., Hogrefe, C., Bessagnet,
857 B., Brandt, J., Christensen, J.H., Chemel, C., Coll, I., van der Gon, H.D., Ferreira, J., Forkel,
858 R., Francis, X.V., Grell, G., Grossi, P., Hansen, A.B., Jericevic, A., Kraljevic, L., Miranda,
859 A.I., Nopmongcol, U., Pirovano, G., Prank, M., Riccio, A., Sartelet, K.N., Schaap, M., Silver,
860 J.D., Sokhi, R.S., Vira, J., Werhahn, J., Wolke, R., Yarwood, G., Zhang, J., Rao, S.T.,
861 Galmarini, S., 2012a. Ensemble modelling of surface level ozone in Europe and North
862 America in the context of AQMEI. *Atmos. Environ.* 53, 60-74.

863 Solazzo, E., Bianconi, R., Pirovano, G., Matthias, V., Vautard, R., Moran, M.D., Appel,
864 K.W., Bessagnet, B., Brandt, J., Christensen, J.H., Chemel, C., Coll, I., Ferreira, J., Forkel,
865 R., Francis, X.V., Grell, G., Grossi, P., Hansen, A.B., Hogrefe, C., Miranda, A.I.,
866 Nopmongco, U., Prank, M., Sartelet, K.N., Schaap, M., Silver, J.D., Sokhi, R.S., Vira, J.,
867 Werhahn, J., Wolke, R., Yarwood, G., Zhang, J., Rao, S.T., Galmarini, S., 2012b.
868 Operational model evaluation for particulate matter in Europe and North America in the
869 context of AQMEII. *Atmos. Environ.* 53, 75-92.

870 Song, C.-K., Byun, D. W., Pierce, R. B., Alsaadi, J. A., Schaack, T. K., and Vukovich, F.:
871 Downscale linkage of global model output for regional chemical transport modeling: method
872 and general performance, *J. Geophys. Res.*, 113, D08308, doi:10.1029/2007JD008951, 2008.

873 Stjern, C. W., Samset, B. H., Myhre, G., Bian, H., Chin, M., Davila, Y., Dentener, F.,
874 Emmons, L., Flemming, J., Haslerud, A. S., Henze, D., Jonson, J. E., Kucsera, T., Lund, M.
875 T., Schulz, M., Sudo, K., Takemura, T., and Tilmes, S.: Global and regional radiative forcing
876 from 20 % reductions in BC, OC and SO₄ – an HTAP2 multi-model study, *Atmos. Chem.*
877 *Phys.*, 16, 13579-13599, <https://doi.org/10.5194/acp-16-13579-2016>, 2016.

878 Tang, Y., Carmichael, G. R., Thongboonchoo, N., Chai, T., Horowitz, L. W., Pierce, R. B.,
879 Al-Saadi, J. A., Pfister, G., Vukovich, J. M., Avery, M. A., Sachse, G. W., Ryerson, T. B.,
880 Holloway, J. S., Atlas, E. L., Flocke, F. M., Weber, R. J., Huey, L. G., Dibb, J. E., Streets, D.
881 G., and Brune, W. H.: Influence of lateral and top boundary conditions on regional air quality
882 prediction: a multiscale study coupling regional and global chemical transport models, *J.*
883 *Geophys. Res.*, 112, D10S18, doi:10.1029/2006JD007515, 2007.

884 United Nations, 2007. Hemispheric transport of air pollution 2007. *Air Pollution Studies No.*
885 16, Interim report prepared by the Task Force on Hemispheric Transport of Air Pollution
886 acting within the framework of the Convention on Long-range Transboundary Air Pollution.
887 New York and Geneva, 2007.

888 Vivanco, M.G., Theobald, M.R., García-Gómez, H., Garrido, J.L., Prank, M., Aas, W.,
889 Adani, M., Alyuz, U., Andersson, C., Bellasio, R., Bessagnet, B., Bianconi, B., Bieser, J.,
890 Brandt, J., Briganti, G., Cappelletti, A., Christensen, J.H., Ciarelli, G., Colette, A., Couvidat,

891 F., Cuvelier, K., D'Isidoro, M., Flemming, J., Fraser, A., Galmarini, S., Geels, C., Hansen,
892 K.M., Hogrefe, C., Im, U., Manders, A., Mircea, M., Pay, M.-T., Pozzoli, L., Raffort, V.,
893 Roustan, Y., Solazzo, E., Tsyro, S., Tuccella, P., Unal, A., Wind, P., 2017. Modelled
894 deposition of nitrogen and sulfur in Europe estimated by 15 air quality models: Evaluation,
895 effects of changes in emissions and implications for habitat protection. In preparation for
896 Atmos. Chem. Phys.

897 Wilkening, K.E., Barrie, L.A., Engle, M., 2000. Atmospheric science: Trans-Pacific air
898 pollution. Science, 290, 65 – 67, doi:10.1126/science.290.5489.65.

899 World Health Organization (WHO), 2013. Review of evidence on health aspects of air
900 pollution (REVIHAAP). WHO Technical Report.

Formatted: English (United States)

901 Table 1. Key features (meteorological/chemistry and transport models, emissions, horizontal and vertical grids) of the regional models
 902 participating to the AQMEII3 health impact study and the perturbation scenarios they performed.

Group Code	Model	Emissions	Horizontal Resolution	Vertical Resolution	Gas Phase	Aerosol Model	Europe				North America			
							BASE	GLO	NAM	EUR	BASE	GLO	EAS	NAM
DE1	COSMO-CLM/CMAQ	HTAP	24 km × 24 km	30 layers, 50 hPa	CB5-TUCL	3 modes	×	×	×	×	×	×	×	×
DK1	WRF/DEHM	HTAP	50 km × 50 km	29 layers, 100 hPa	Brandt et al. (2012)	2 modes	×	×	×	×	×	×	×	×
ES1	WRF/CHEM	MACC	23 km × 23 km	33 layers, 50 hPa	RADM2	3 modes, MADE/SORGAM	×		×					
FI1	ECMWF/SILAM	MACC+HTAP	0.25° × 0.25°	12 layers, 13 km	CB4	1-5 bins, VBS	×	×	×	×				
FRES1	ECMWF/CHIMERE	HTAP+HTAP	0.25° × 0.25°	9 layers, 50 hPa	MELCHIOR2	8 bins	×	×	×	×				
IT1	WRF/CHEM	MACC	23 km × 23 km	33 layers, 50 hPa	RACM-ESRL	3 modes, MADE/VBS	×	×		×				
IT2	WRF/CAMx	MACC	23 km × 23 km	14 layers, 8 km	CB5	3 modes	×	×						
NL1	LOTOS/EUROS	MACC	0.50° × 0.25°	4 layers, 3.5 km	CB4	2 modes, VBS	×							
TR1	WRF/CMAQ	MACC	30 km × 30 km	24 layers, 10hPa	CB5	3 modes	×	×	×					
UK1	WRF/CMAQ	MACC	15 km × 15 km	23 layers, 100 hPa	CB5-TUCL	3 modes	×	×	×	×				
UK2	WRF/CMAQ	HTAP	30 km × 30 km	23 layers, 100 hPa	CB5-TUCL	3 modes	×	×						
UK3	WRF/CMAQ	MACC	18 km × 18 km	35 layers, 16 km	CB5	3 modes	×	×	×					
US3	WRF/CMAQ	SMOKE	12 km × 12 km	35 layers, 50 hPa	CB5-TUCL	3 modes					×	×	×	×

903

904 ¹ MACC: Modelling group used only the MACC emissions, MACC+HTAP: Modelling group used MACC emissions for Europe and HTAP
 905 emissions over North Africa.

906

Formatted Table

Formatted Table

907 Table 2. Perturbations of global/regional anthropogenic emissions and boundary conditions in the perturbation scenarios.

	GLO	Europe		North America	
		NAM	EUR	NAM	EAS
Emissions	-20%	-	-20%	-20%	-
Boundary conditions (Emissions in the IFS model)	-20%	-20%	-20%	-20%	-20%

908

909

910 Table 3. Monthly statistics of Pearson's Correlation (*r*), Normalized Mean Bias (*NMB*:%), Normalized Mean Gross Error (*NMGE*:%) and Root
 911 Mean Square Error (*RMSE*: $\mu\text{g m}^{-3}$ for Europe, while ppb for gases and $\mu\text{g m}^{-3}$ for particles for North America) calculated for each model group.

		EUROPE												NORTH AMERICA							
		DE1	DK1	ES1	FI1	FRES1	IT1	IT2	TR1	UK1	UK2	MEAN	MEDIAN	C-IFS	DE1	DK1	US1	US3	MEAN	MEDIAN	C-IFS
O ₃	r	0.63	0.90	0.82	0.83	0.91	0.92	0.93	0.87	0.92	0.90	0.93	0.92	0.89	0.78	0.59	0.89	0.87	0.84	0.83	0.71
	NMB	0.10	0.07	-0.14	-0.36	-0.10	0.04	-0.14	0.09	0.08	-0.03	-0.04	-0.04	-0.20	0.12	0.22	0.14	-0.02	0.09	0.11	-0.10
	NMGE	0.17	0.12	0.15	0.36	0.12	0.13	0.15	0.26	0.11	0.09	0.08	0.08	0.20	0.17	0.23	0.14	0.08	0.12	0.13	0.19
	RMSE	12.68	8.81	11.58	23.13	9.01	8.54	10.94	17.66	8.05	6.79	5.91	6.31	14.63	6.16	9.81	5.72	3.23	4.63	5.28	7.31
NO ₂	r	0.80	0.88	0.89	0.95	0.74	0.90	0.92	0.90	0.85	0.85	0.95	0.93	0.92	0.99	0.92	0.94	0.93	0.98	0.99	0.91
	NMB	-0.75	-0.38	-0.47	0.00	0.05	-0.29	-0.30	0.58	-0.32	-0.06	-0.17	-0.24	0.07	-0.18	-0.35	0.05	0.31	-0.03	-0.02	0.41
	NMGE	0.75	0.38	0.47	0.20	0.23	0.29	0.30	0.58	0.32	0.17	0.18	0.24	0.20	0.18	0.35	0.10	0.31	0.06	0.02	0.41
	RMSE	9.38	5.41	6.00	2.89	3.44	4.43	4.15	7.39	4.65	2.74	2.70	3.49	2.59	1.01	2.05	0.62	1.77	0.40	0.26	2.30
CO	r	0.83	0.76	0.74	0.88	0.82	0.84	0.79	0.87	0.63	0.72	0.92	0.84	0.91	0.79	0.74	0.74	0.73	0.88	0.82	0.80
	NMB	-0.42	-0.42	-0.44	-0.27	-0.32	-0.38	-0.44	-0.20	-0.41	-0.43	-0.33	-0.38	-0.25	-0.19	-0.07	-0.06	-0.04	-0.07	-0.07	0.17
	NMGE	0.42	0.42	0.44	0.27	0.32	0.38	0.44	0.21	0.41	0.43	0.33	0.38	0.25	0.19	0.11	0.08	0.08	0.08	0.07	0.17
	RMSE	128.62	134.31	132.78	89.99	107.81	128.14	135.83	70.04	130.21	135.82	106.98	123.61	84.73	40.27	24.90	22.44	20.51	19.94	20.41	37.30
SO ₂	r	0.85	0.90	0.88	0.86	0.87	0.86	0.86	0.54	0.83	0.83	0.93	0.92	0.70	0.79	0.81	0.80	0.78	0.87	0.78	0.04
	NMB	-0.01	-0.47	-0.65	-0.20	-0.16	-0.30	-0.55	0.04	-0.13	0.20	-0.19	-0.10	0.41	-0.46	-0.42	0.07	-0.13	-0.19	-0.13	0.35
	NMGE	0.24	0.48	0.65	0.28	0.22	0.31	0.55	0.28	0.19	0.28	0.21	0.12	0.45	0.46	0.42	0.11	0.13	0.19	0.13	0.35
	RMSE	0.92	1.47	2.03	0.95	0.80	1.23	1.71	1.14	0.86	1.05	0.76	0.58	1.39	1.27	1.18	0.32	0.40	0.53	0.40	1.02
PM ₁₀	r	0.86	0.82	0.17	0.41	0.82	0.60	0.10	0.52	0.71	0.71	0.87	0.73	-0.74	-0.31	-0.47	NA	0.07	0.47	-0.07	0.02
	NMB	-0.71	-0.59	-0.47	-0.42	-0.51	-0.20	-0.48	-0.25	-0.47	-0.42	-0.41	-0.45	-0.62	-0.67	-0.84	NA	-0.25	-0.44	-0.46	-0.86
	NMGE	0.71	0.59	0.47	0.42	0.51	0.25	0.48	0.26	0.47	0.42	0.41	0.45	0.62	0.67	0.84	NA	0.27	0.44	0.46	0.86
	RMSE	20.43	18.25	16.16	14.67	15.74	9.78	16.48	10.45	14.78	13.72	13.15	14.63	19.87	20.42	25.09	NA	9.85	13.51	14.74	25.58
PM _{2.5}	r	0.89	0.86	0.24	0.58	0.84	0.75	0.11	0.62	0.77	0.77	0.89	0.82	-0.73	0.52	0.02	NA	0.54	0.61	0.56	0.18
	NMB	-0.64	-0.47	-0.27	-0.27	-0.36	-0.19	-0.48	-0.17	-0.40	-0.28	-0.32	-0.33	-0.59	-0.63	-0.14	NA	0.17	-0.15	-0.08	-0.39
	NMGE	0.64	0.47	0.35	0.30	0.36	0.24	0.49	0.24	0.41	0.30	0.32	0.33	0.59	0.63	0.20	NA	0.22	0.15	0.11	0.40
	RMSE	11.95	9.92	9.20	8.02	8.06	6.57	11.65	6.82	8.65	7.15	7.51	7.99	12.97	6.79	2.40	NA	2.78	1.92	1.41	5.04

915 Table 5. Annual mean absolute differences (ppb for gases and $\mu\text{g m}^{-3}$ for particles) between the base case and the different emission perturbation
 916 scenarios as calculated by the different model groups over the North American domain.

Pollutant	Scenario	DE1	DK1	US1	US3	All Mean	Common Mean
O ₃	GLO	-1.70	-1.42	-1.41	-1.03	-1.39	-1.39
	NAM	-0.92	-0.66		-0.36	-0.65	-0.65
	EAS	-0.35	-0.24	-0.23	-0.19	-0.25	-0.26
NO ₂	GLO	-0.35	-0.63	-1.07	-1.20	-0.81	-0.73
	NAM	-0.36	-0.62		-1.17	-0.71	-0.71
	EAS	0.00	0.00	0.00	-0.01	0.00	0.00
CO	GLO	-9.31	-20.48	-22.12	-25.01	-19.23	-18.27
	NAM	-3.84	-13.35		-19.87	-12.35	-12.35
	EAS	-2.60	-4.16	-3.64	-3.07	-3.37	-3.28
SO ₂	GLO	-0.33	-0.32	-0.48	-0.25	-0.34	-0.30
	NAM	-0.33	-0.32		-0.48	-0.37	-0.37
	EAS	0.00	0.00		0.00	0.00	0.00
PM ₁₀	GLO	-2.26	-0.66		-4.24	-2.39	-2.39
	NAM	-2.02	-0.59		-4.19	-2.27	-2.27
	EAS	-0.56	-0.05		-0.03	-0.21	-0.21
PM _{2.5}	GLO	-0.60	-1.67		-2.29	-1.52	-1.52
	NAM	-0.62	-1.56		-2.24	-1.47	-1.47
	EAS	0.01	-0.04		-0.03	-0.02	-0.02

917

918

919 Table 6. Annual mean RERER values calculated for the multi-model mean ensembles over Europe and North America.

	O ₃	NO ₂	CO	SO ₂	PM ₁₀	PM _{2.5}
EUROPE						
DE1	0.44	-0.09	0.44	0.02	0.01	0.01
DK1	0.85	0.23	0.63	0.37	0.17	0.28
FI1	0.76	-0.01	0.40	0.01	0.02	0.02
FRES1	0.78	0.15	0.56	0.30	0.20	0.20
IT1	1.10	0.34	0.93	0.42	0.27	0.26
UK1	0.92	0.35	0.52	0.43	0.33	0.34
MMM	0.77	0.18	0.55	0.27	0.18	0.19
NORTH AMERICA						
DE1	0.77	0.12	0.73	0.07	0.09	0.12
DK1	0.93	0.06	0.90	0.15	0.07	0.12
US3	0.54	0.02	0.47	0.11	0.08	0.10
MMM	0.75	0.05	0.71	0.11	0.08	0.11

	O ₃	NO ₂	CO	SO ₂	PM ₁₀	PM _{2.5}
EUROPE						
DE1	0.44	-0.09	0.44	0.02	0.01	0.01
DK1	0.85	0.23	0.63	0.37	0.17	0.28
FI1	0.76	-0.01	0.40	0.01	0.02	0.02
FRES1	0.78	0.15	0.56	0.30	0.20	0.20
IT1	1.10	0.34	0.93	0.42	0.27	0.26
UK1	0.92	0.35	0.52	0.43	0.33	0.34
MMM	0.77	0.18	0.55	0.27	0.18	0.19
MEDIAN	0.81	0.19	0.54	0.34	0.18	0.23
NORTH AMERICA						

Formatted: English (United States)

Formatted: Font: (Default) Times New Roman, 12 pt

Formatted: Font: (Default) Times New Roman, 12 pt, Subscript

Formatted: Font: (Default) Times New Roman, 12 pt

Formatted: Font: (Default) Times New Roman, 12 pt, Subscript

Formatted: Font: (Default) Times New Roman, 12 pt

Formatted: Font: (Default) Times New Roman, 12 pt, Subscript

Formatted: Font: (Default) Times New Roman, 12 pt

Formatted: Font: (Default) Times New Roman, 12 pt, Subscript

Formatted: Font: (Default) Times New Roman, 12 pt

Formatted: Font: (Default) Times New Roman, 12 pt, Subscript

Formatted: Font: (Default) Times New Roman, 12 pt

Formatted: English (United States)

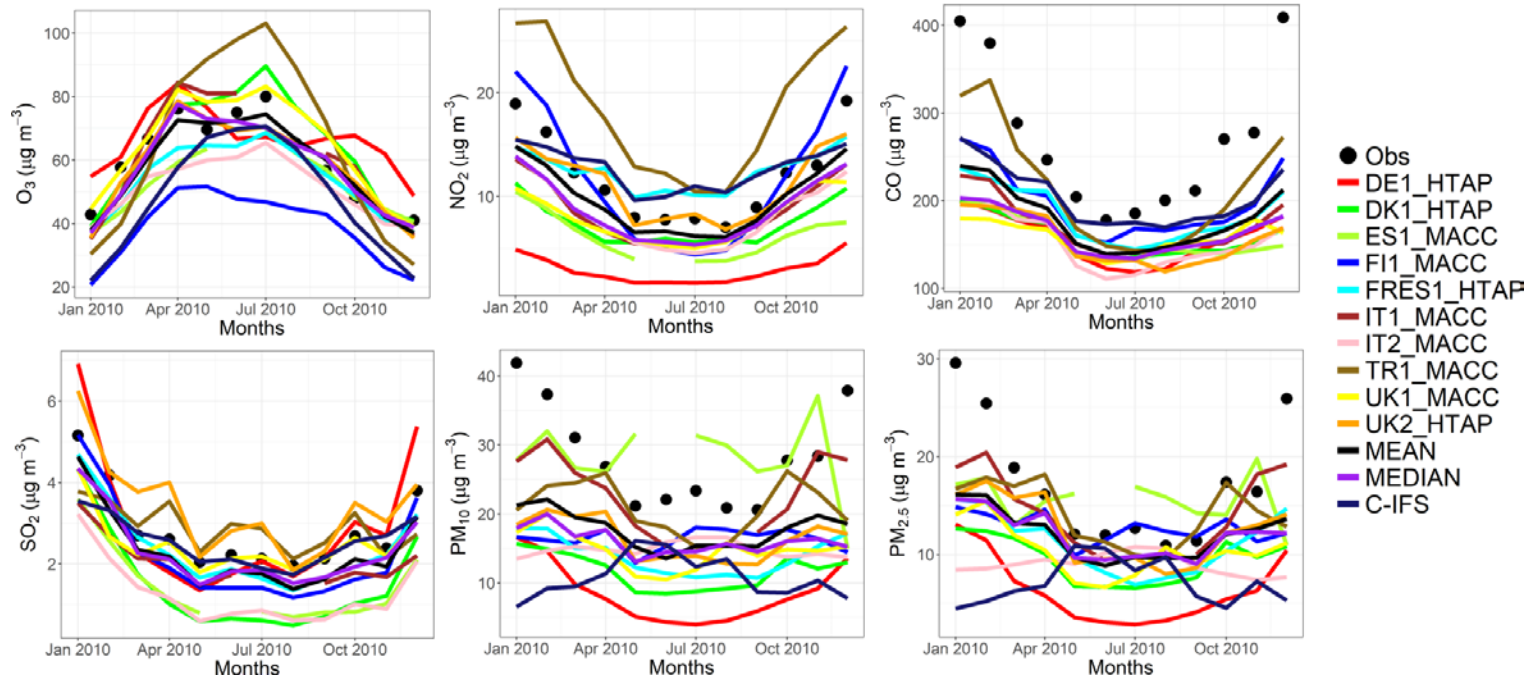
Formatted Table

Formatted: Font: (Default) Times New Roman, 12 pt

920

<u>DE1</u>	<u>0.77</u>	<u>0.12</u>	<u>0.73</u>	<u>0.07</u>	<u>0.09</u>	<u>0.12</u>
<u>DK1</u>	<u>0.93</u>	<u>0.06</u>	<u>0.90</u>	<u>0.15</u>	<u>0.07</u>	<u>0.12</u>
<u>US3</u>	<u>0.54</u>	<u>0.02</u>	<u>0.47</u>	<u>0.11</u>	<u>0.08</u>	<u>0.10</u>
<u>MMM</u>	<u>0.75</u>	<u>0.05</u>	<u>0.71</u>	<u>0.11</u>	<u>0.08</u>	<u>0.11</u>
<u>MEDIAN</u>	<u>0.77</u>	<u>0.06</u>	<u>0.73</u>	<u>0.11</u>	<u>0.08</u>	<u>0.12</u>

Formatted: Font: (Default) Times New Roman, 12 pt

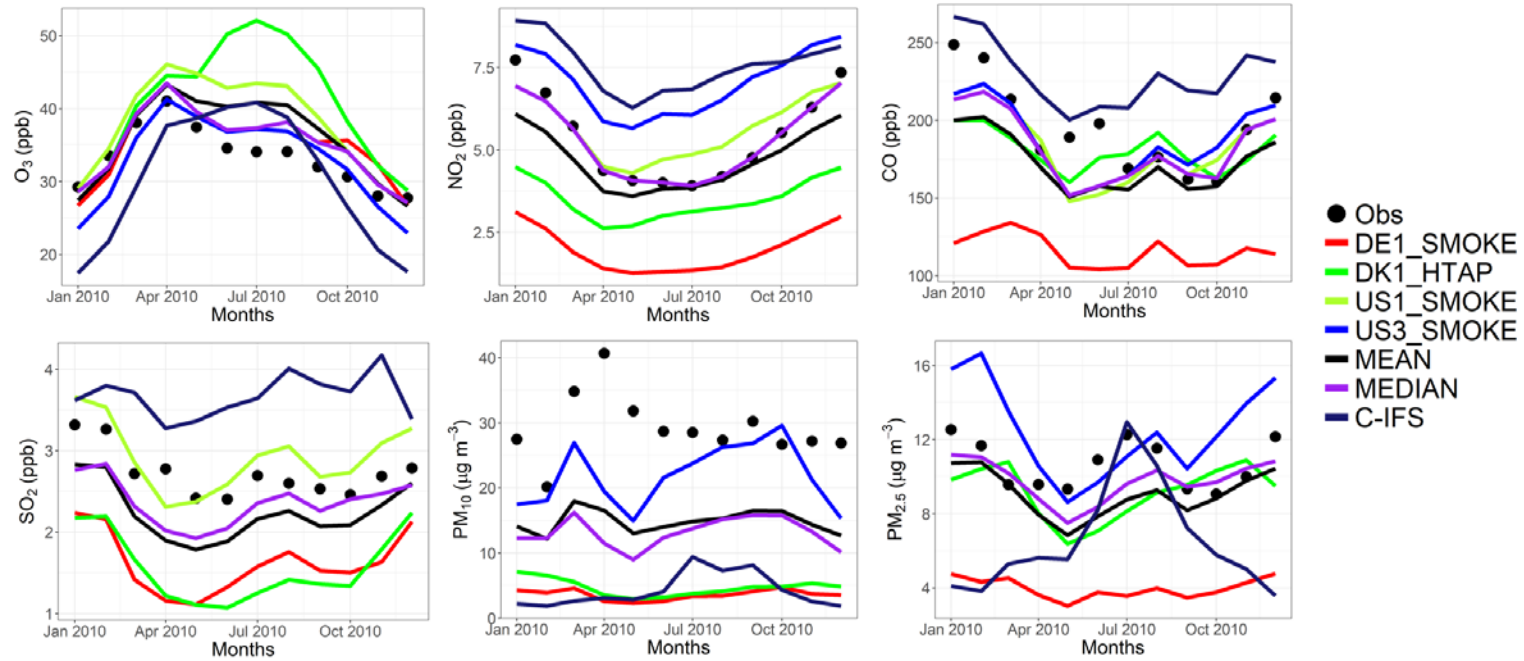


922

923 Fig.1. Observed and simulated monthly mean air pollutant levels, averaged over the monitoring stations over Europe.

924

925

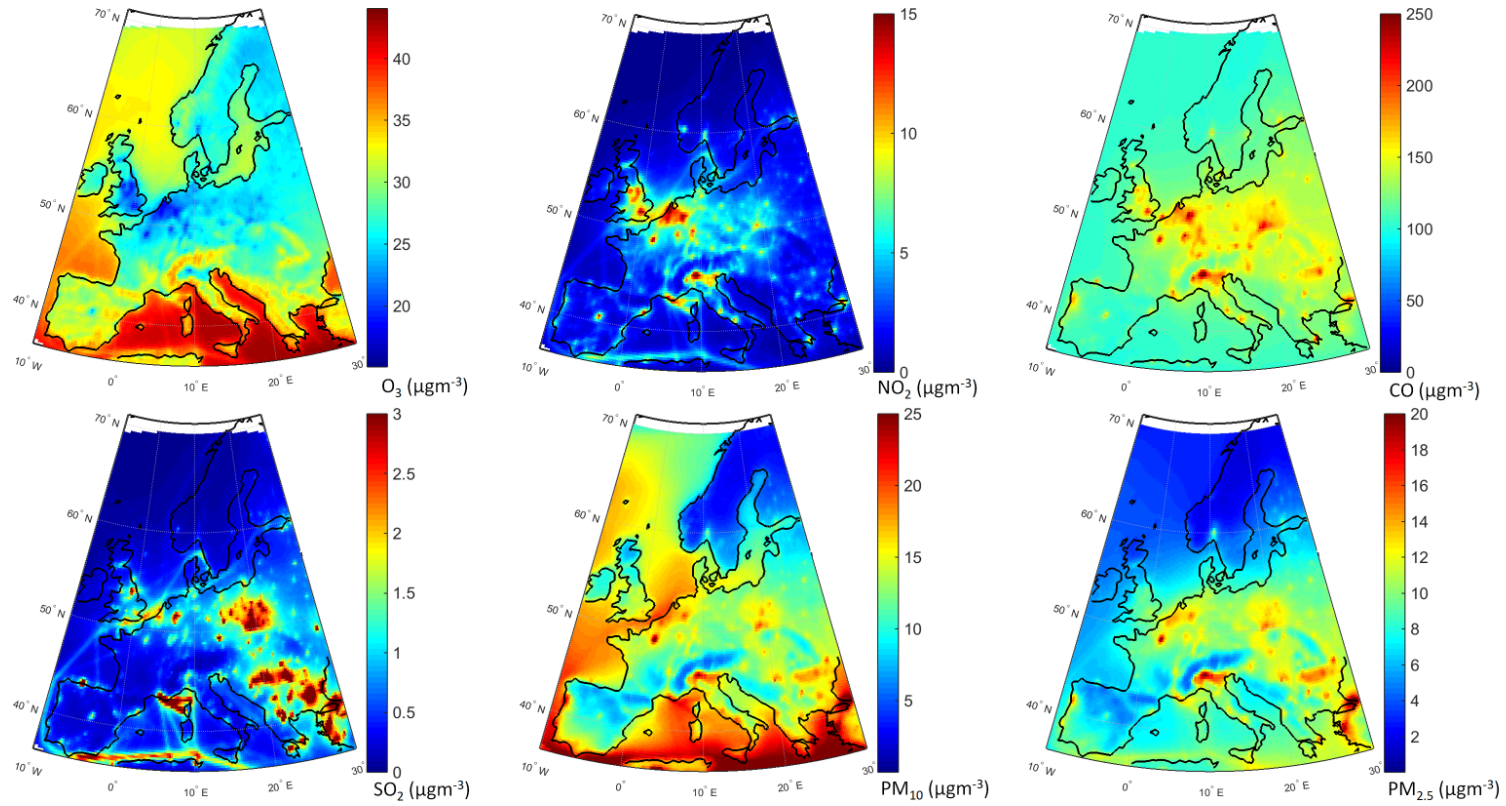


926

927 Fig.2. Observed and simulated monthly mean air pollutant levels, averaged over the monitoring stations over North America.

928

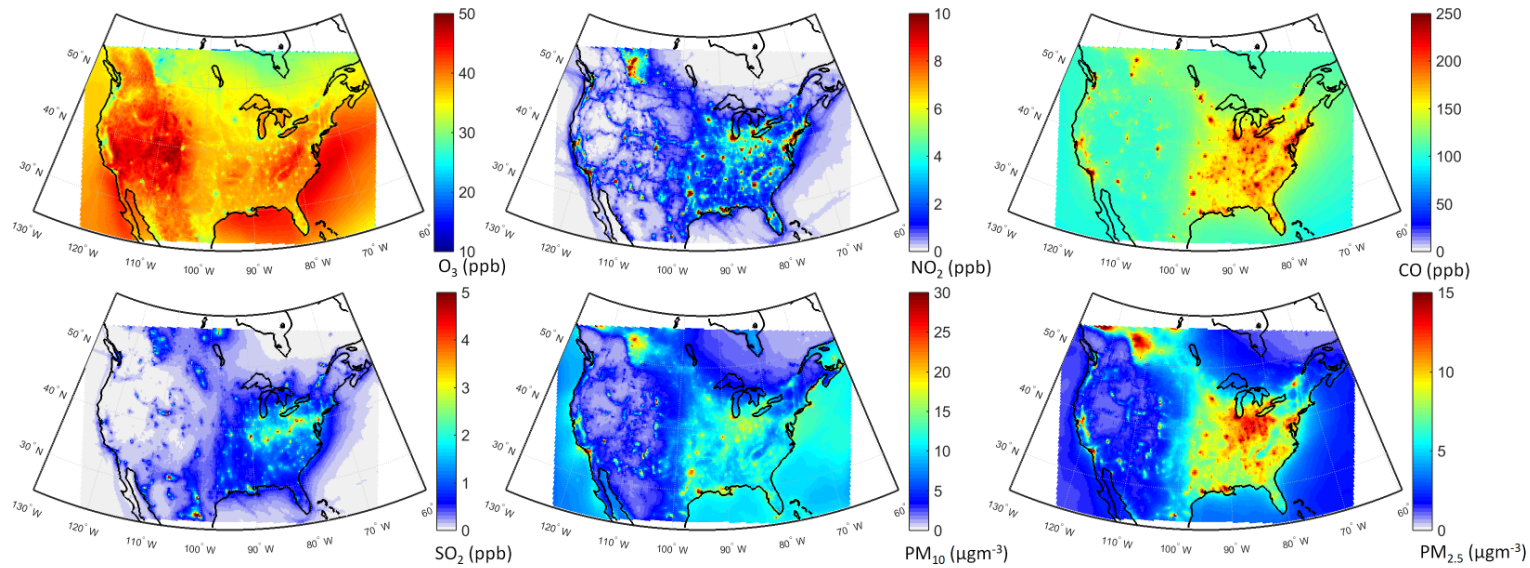
929



930

931 Fig.3. Multi-model mean air pollutant levels over Europe as simulated in the base case.

932



933 Fig.4. Multi-model mean air pollutant levels over North America as simulated in the base case.
 934

935

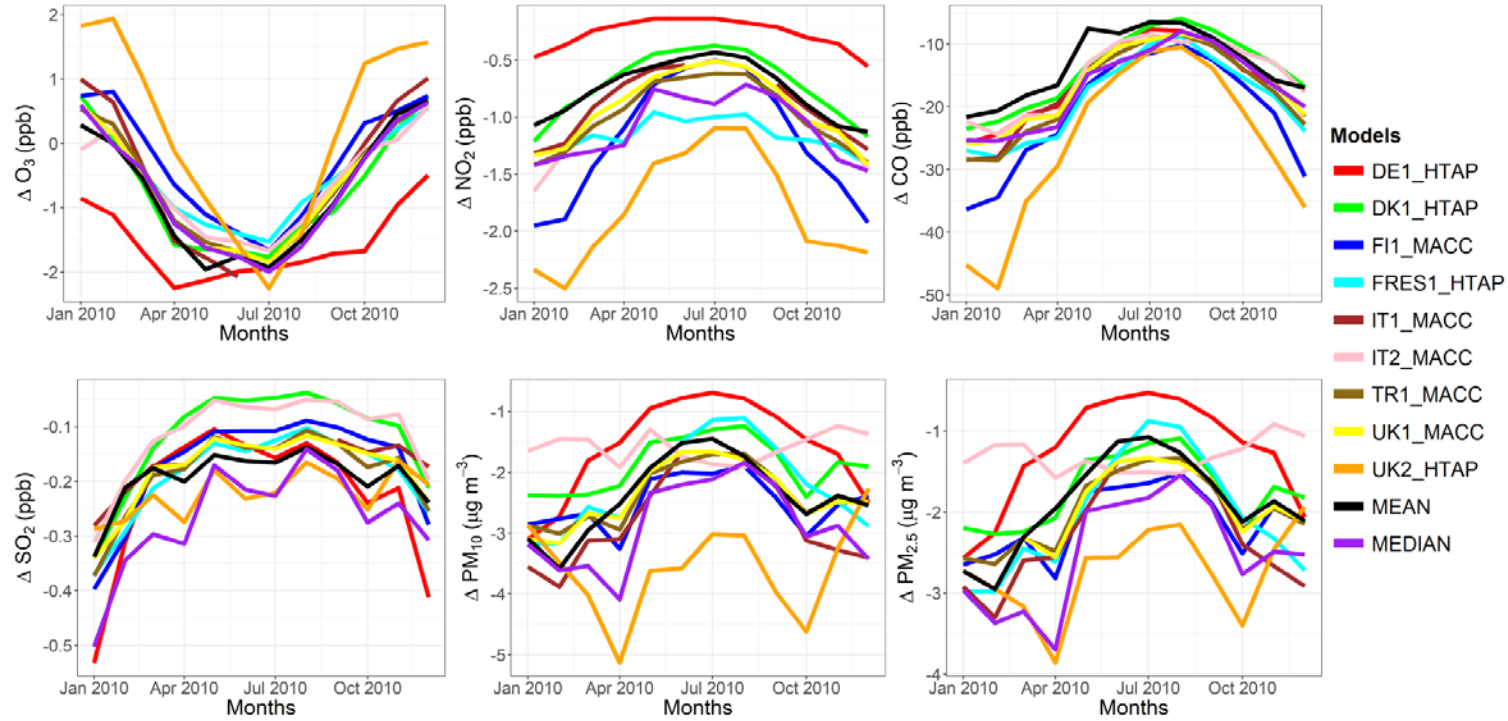
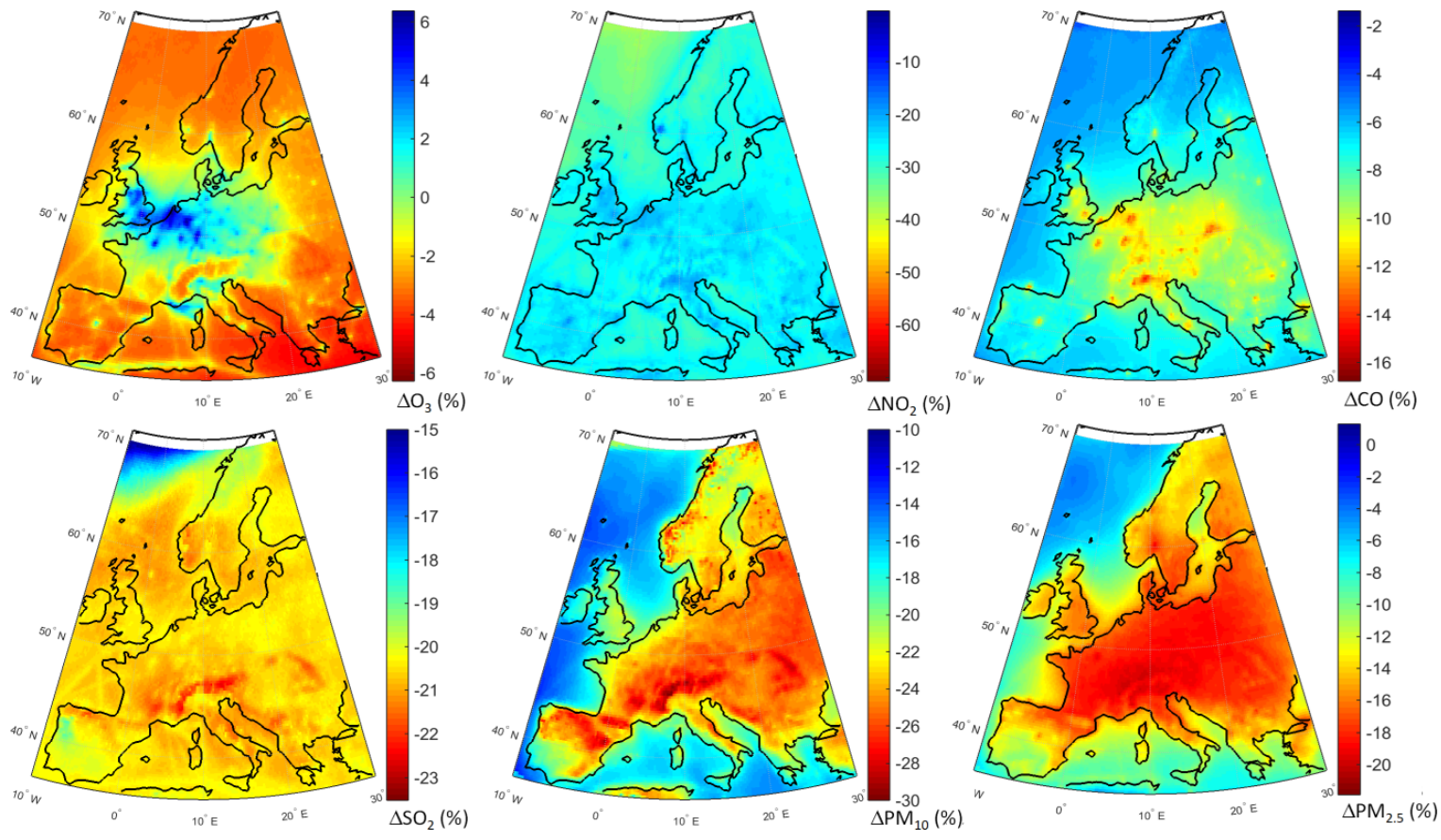


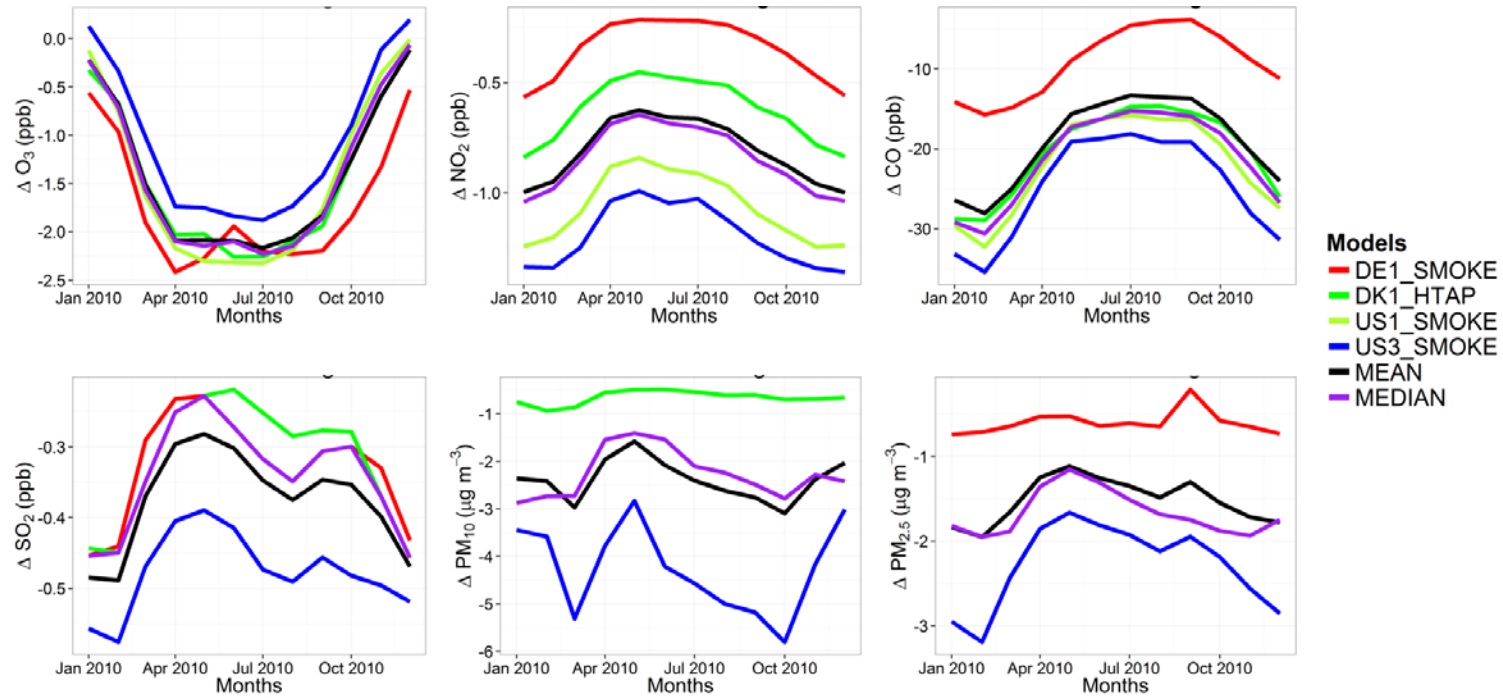
Fig.5. Absolute impact of the 20% reduction of the global anthropogenic emissions over Europe (GLO_{EUR}-BASE_{EUR}).



940

941 Fig.6. Spatial distribution of the annual mean relative differences between the global perturbation scenario and the base case over Europe as
 942 simulated by the multi-model mean ensemble.

943

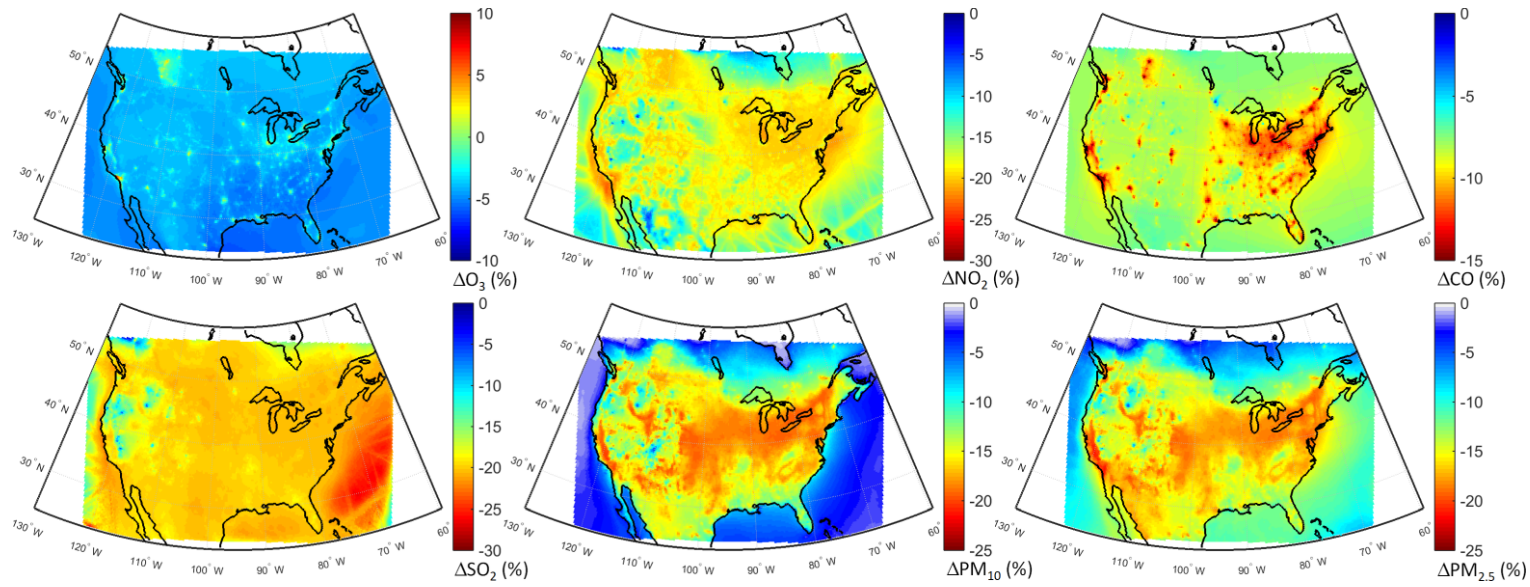


944

945

Fig.7. Absolute impact of the 20% reduction of the global anthropogenic emissions over North America (GLO_{NAM}-BASE_{NAM}).

946

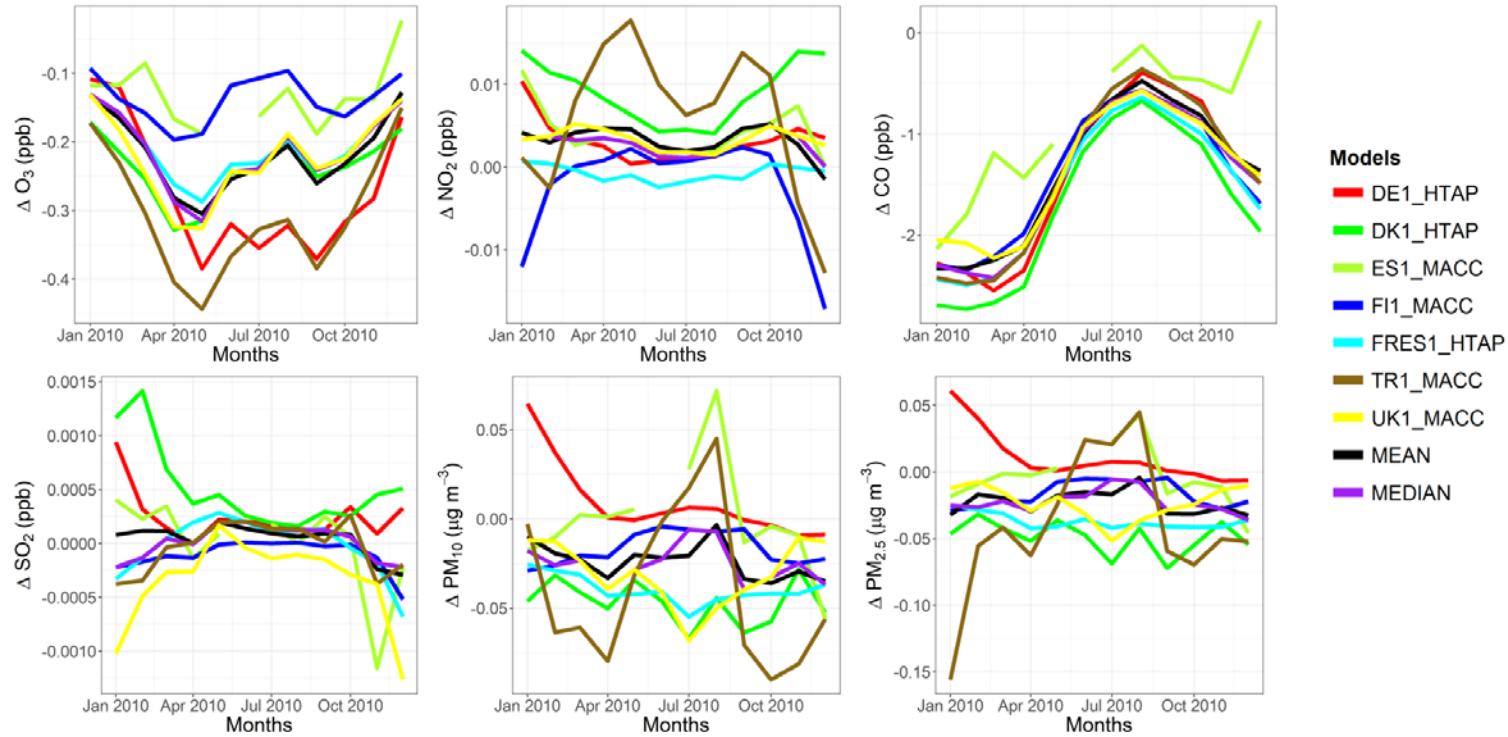


947

948 Fig.8. Spatial distribution of the annual mean relative differences between the global perturbation scenario and the base case over North America
 949 as simulated by the multi-model mean ensemble.

950

951

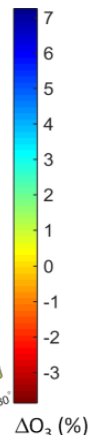
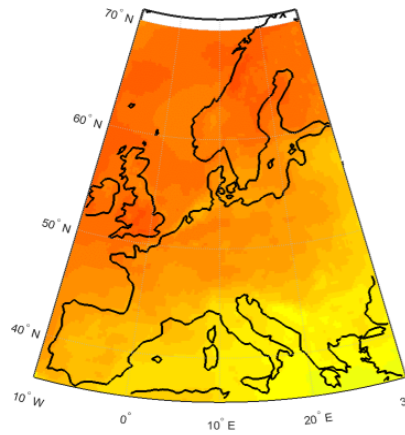


952

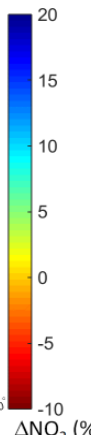
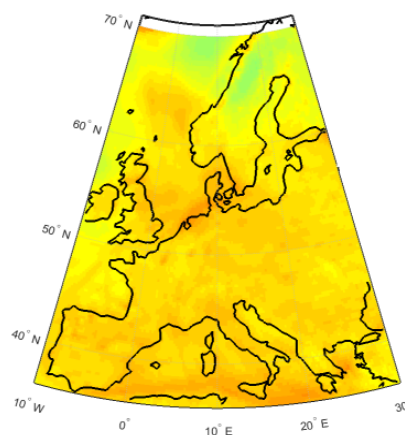
953

Fig.9. Absolute impact of the 20% reduction of the North American anthropogenic emissions over Europe (NAM_{EUR}-BASE_{EUR}).

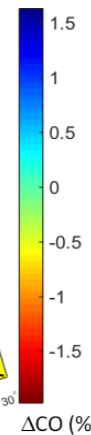
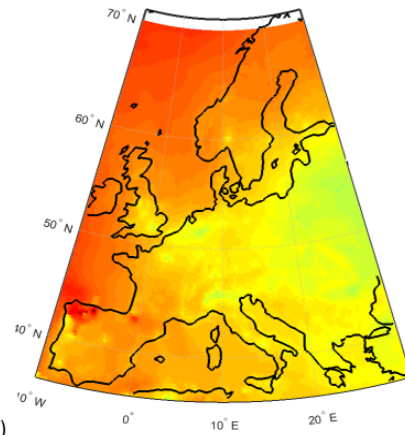
954



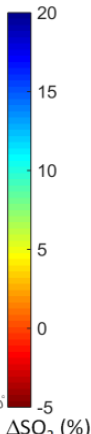
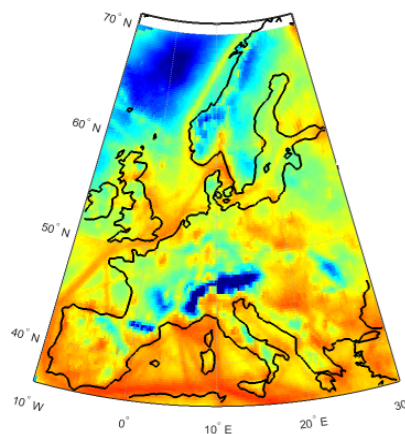
ΔO_3 (%)



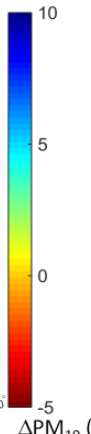
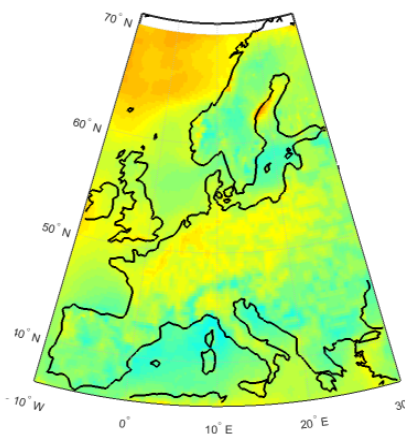
ΔNO_2 (%)



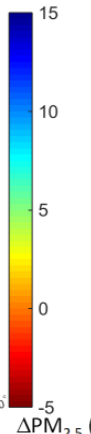
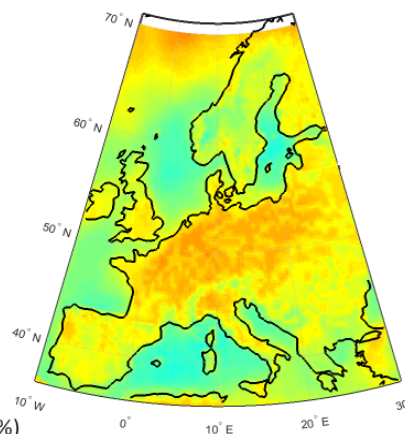
ΔCO (%)



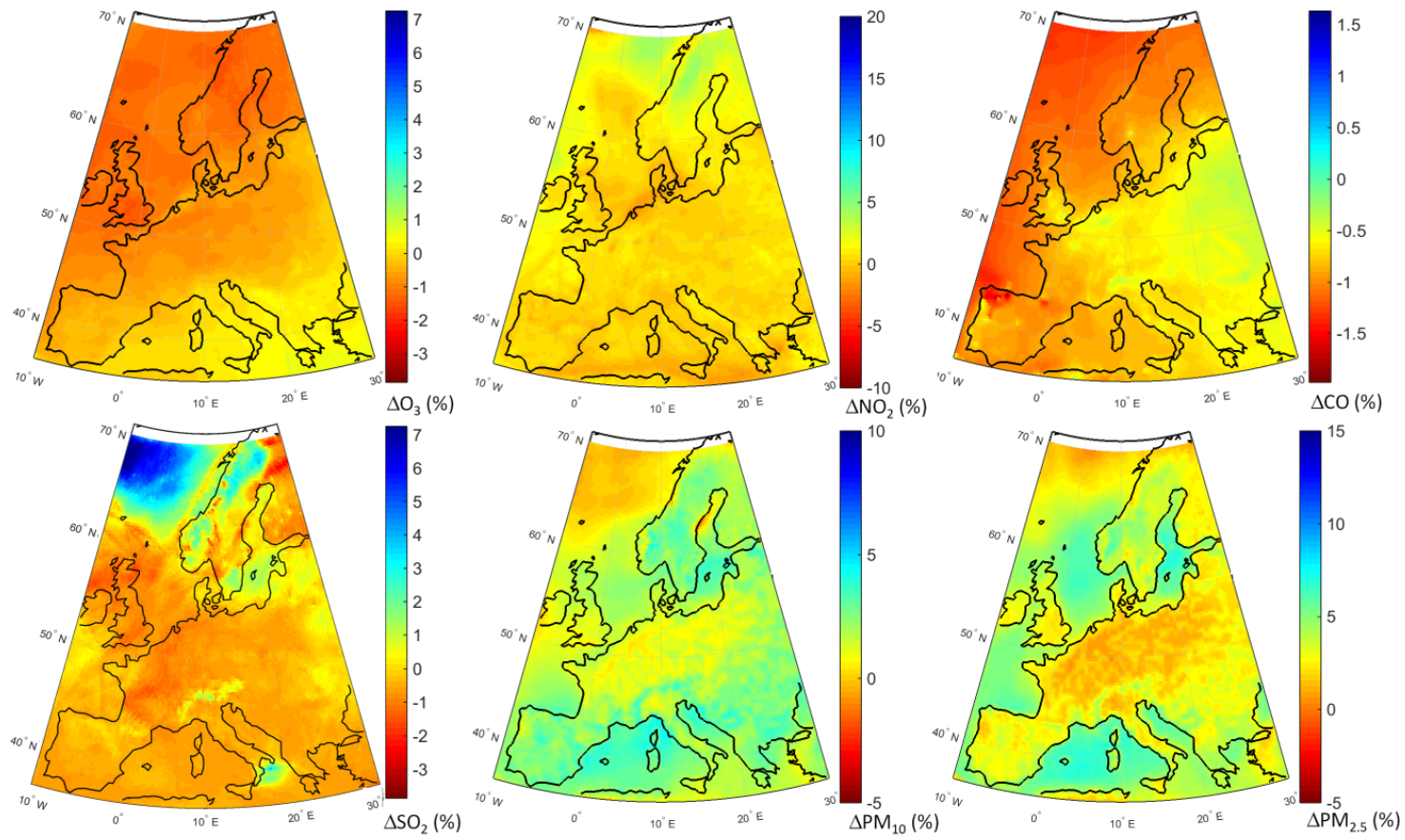
ΔSO_2 (%)



ΔPM_{10} (%)

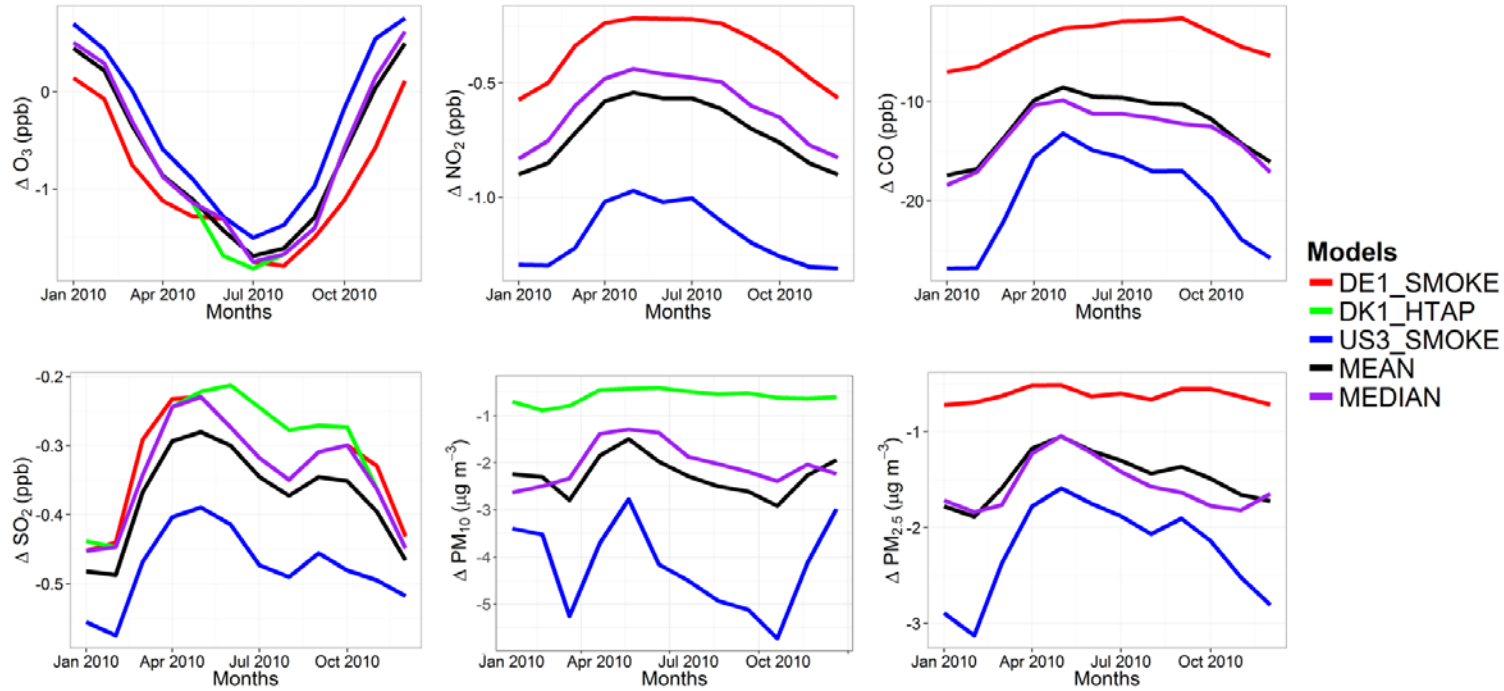


$\Delta PM_{2.5}$ (%)

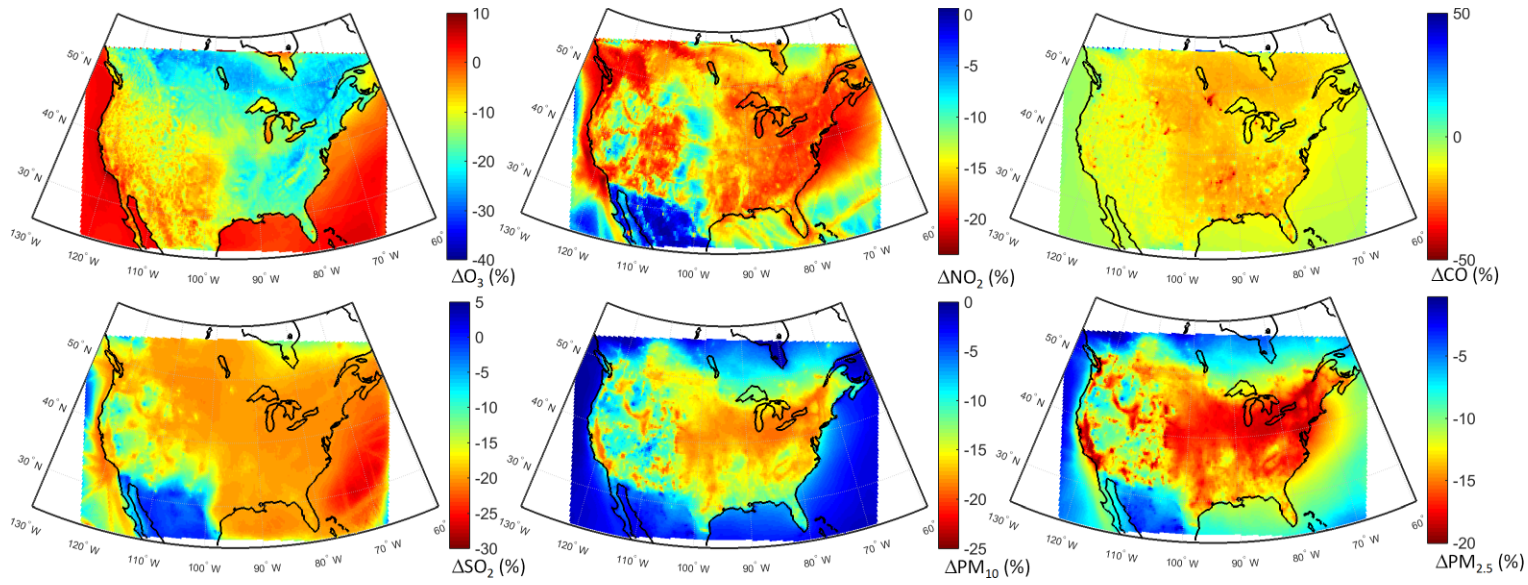


956

957 Fig.10. Spatial distribution of the annual mean relative differences between the North American emissions perturbation scenario and the base
 958 case over Europe as simulated by the multi-model mean ensemble.



960 Fig.11. Absolute impact of the 20% reduction of the North American anthropogenic emissions over North America (GLO_{NAM}-BASE_{NAM}).
 961

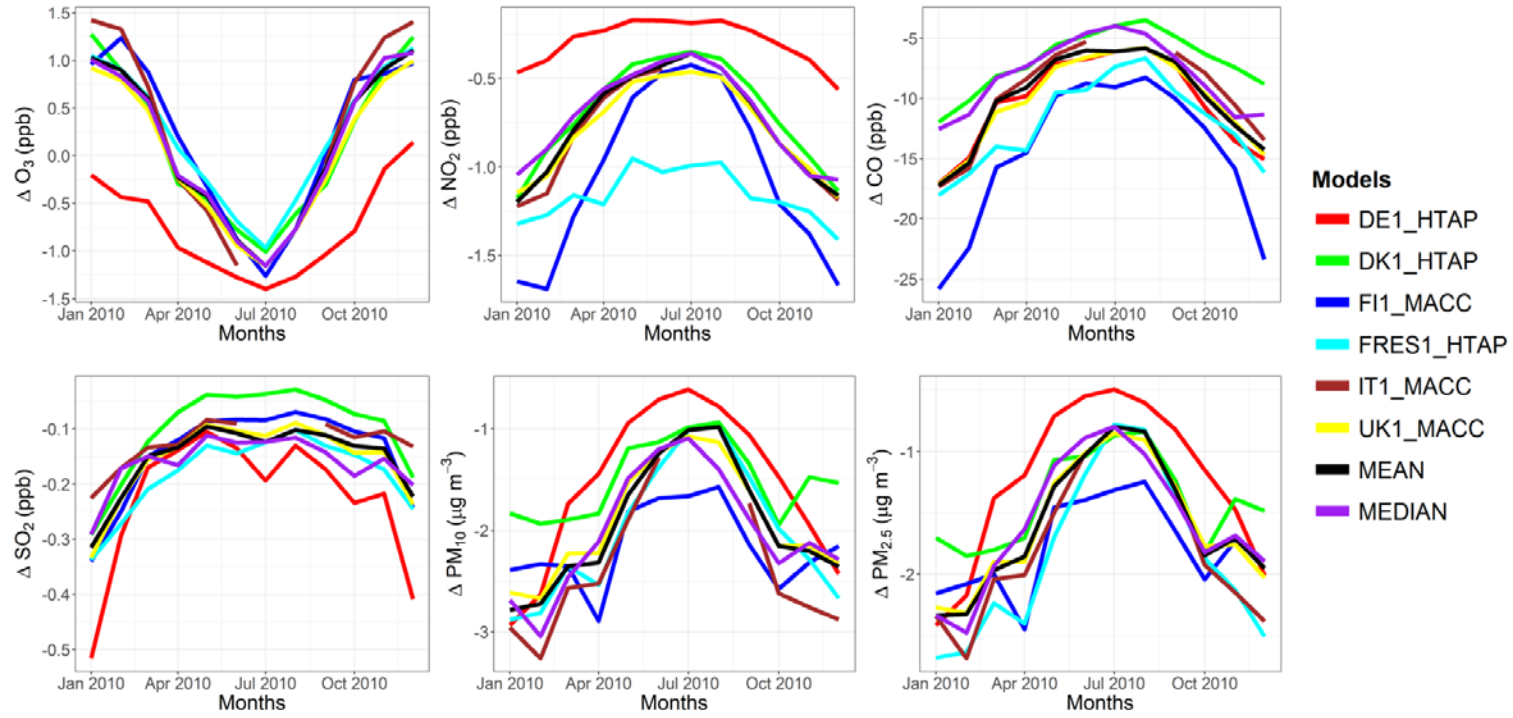


964

965 Fig.12. Spatial distribution of the annual mean relative differences between the North American emissions perturbation scenario and the base
 966 case over North America as simulated by the multi-model mean ensemble.

967

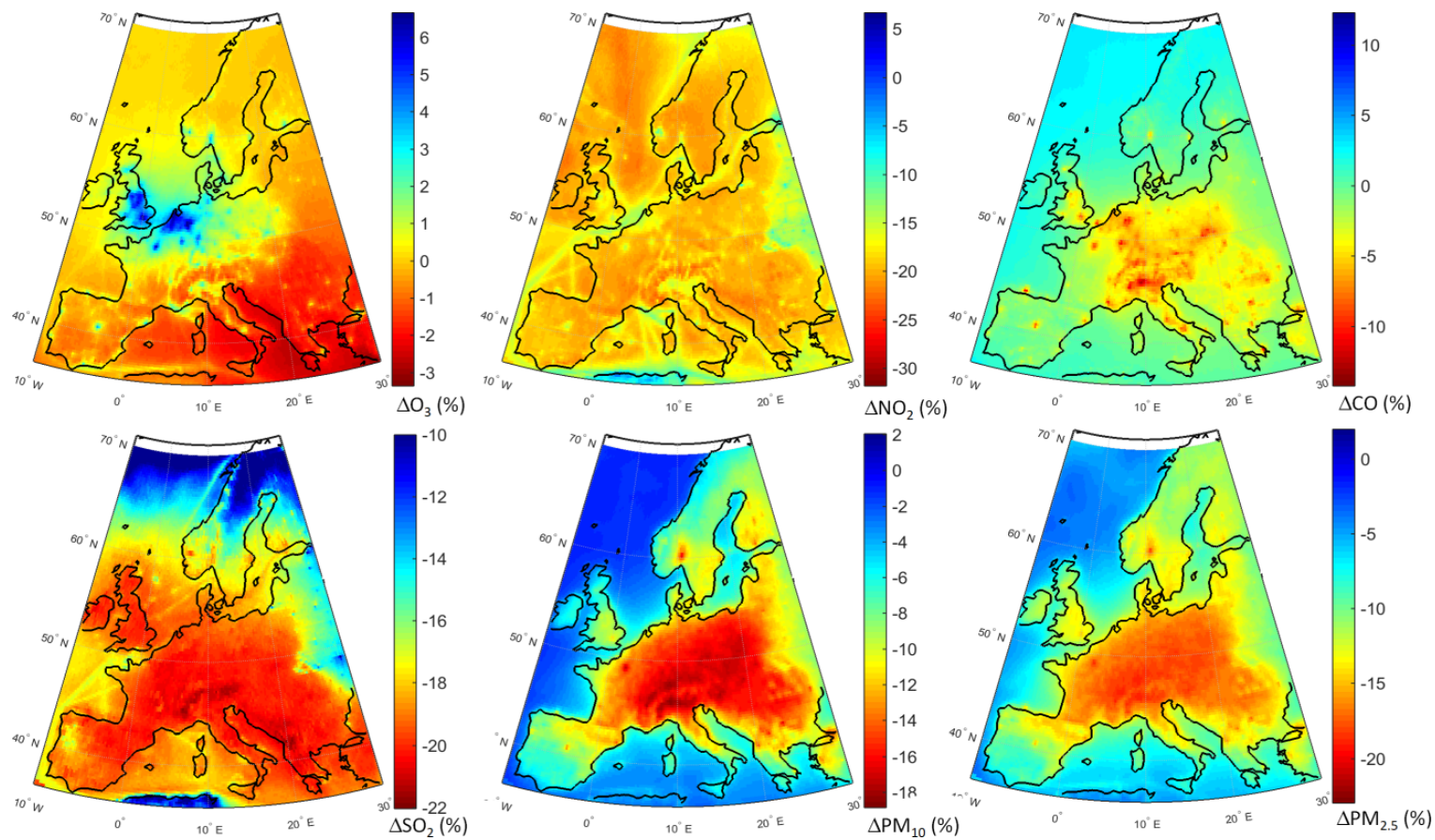
968



969

970 Fig.13. Absolute impact of the 20% reduction of the European anthropogenic emissions over Europe (EUR_{EUR}-BASE_{EUR}).

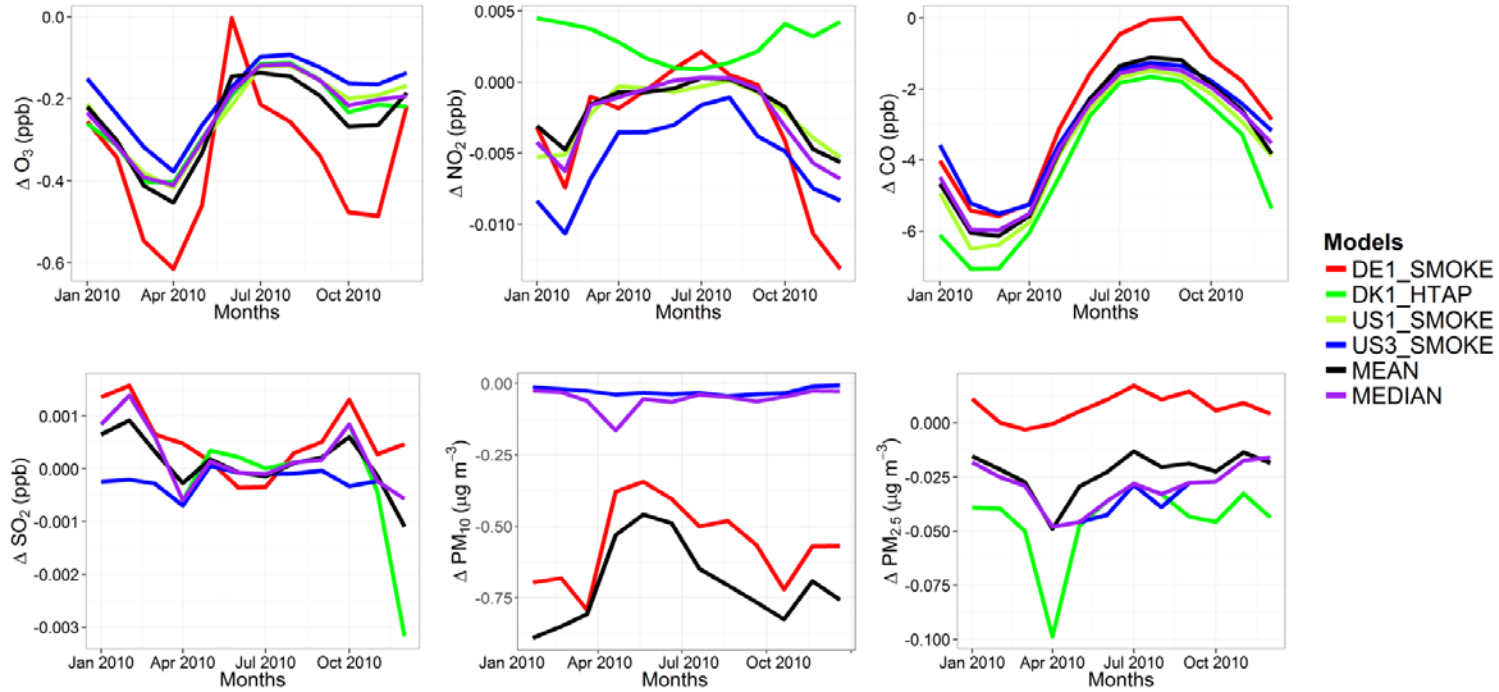
971



972

973 Fig.14. Spatial distribution of the annual mean relative differences between the European emissions perturbation scenario and the base case over
 974 Europe as simulated by the multi-model mean ensemble.

975



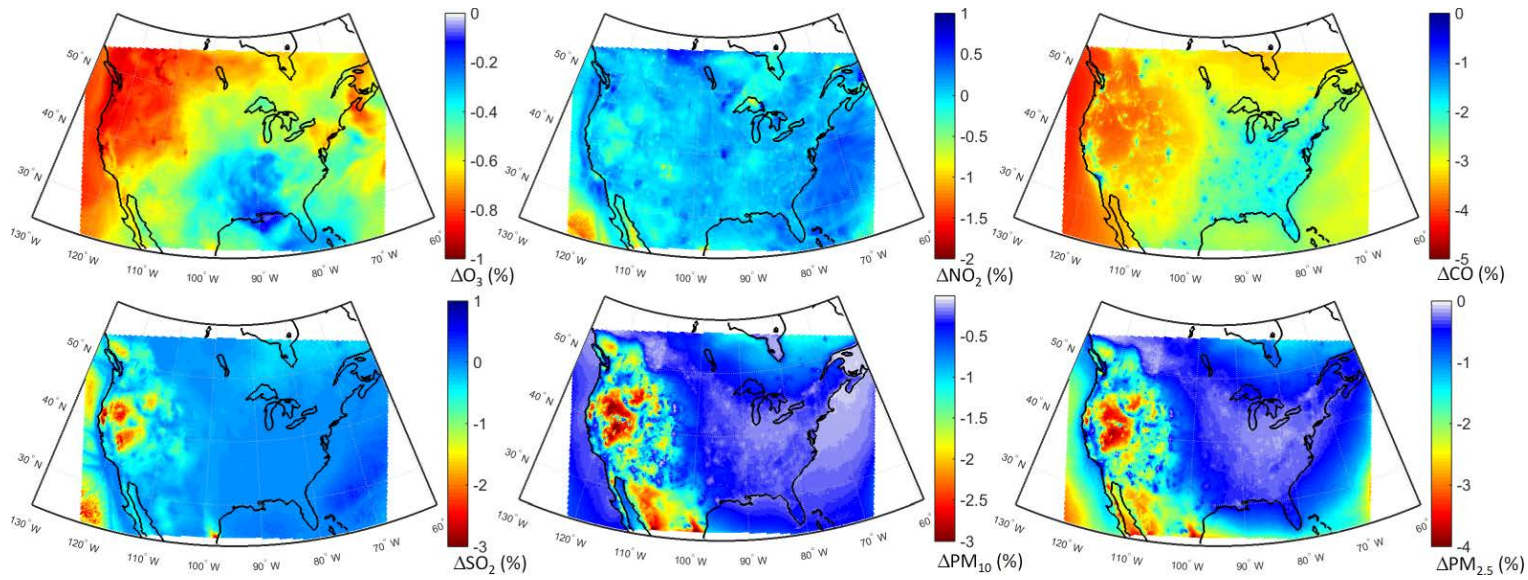
976

977 Fig.15. Absolute impact of the 20% reduction of the East Asian anthropogenic emissions over North America (GLONAM-BASE_{NAM}).

978

979

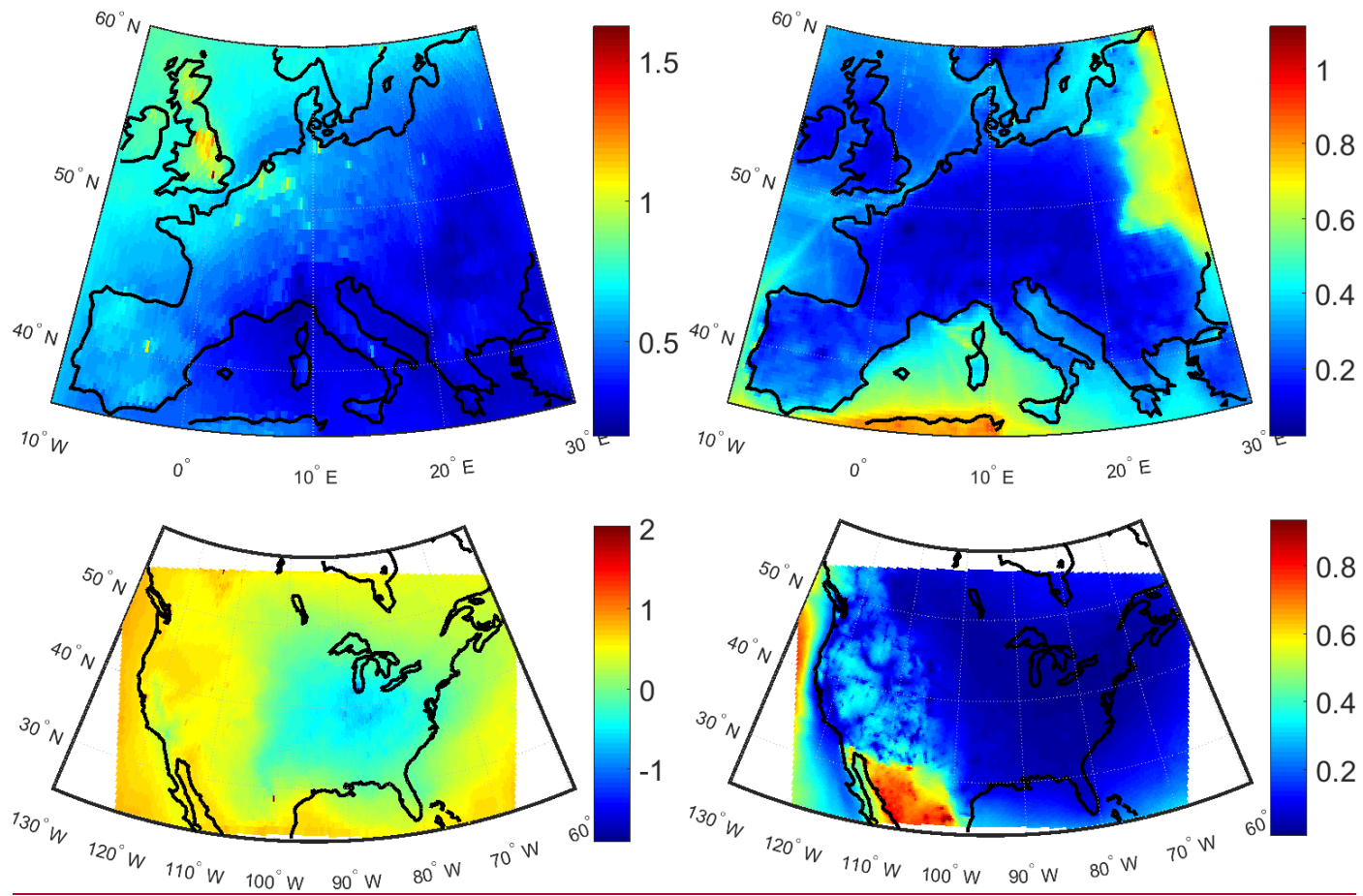
980



981

982 Fig. 16. Spatial distribution of the annual mean relative differences between the East Asian emissions perturbation scenario and the base case
 983 over North America as simulated by the multi-model mean ensemble.

984



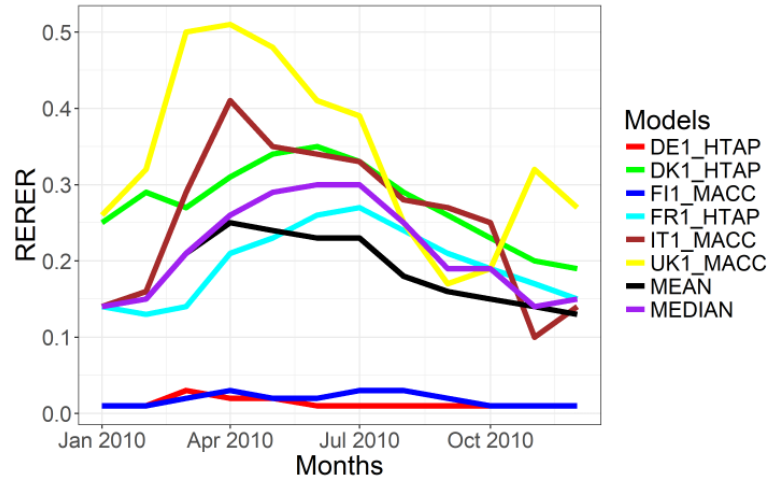
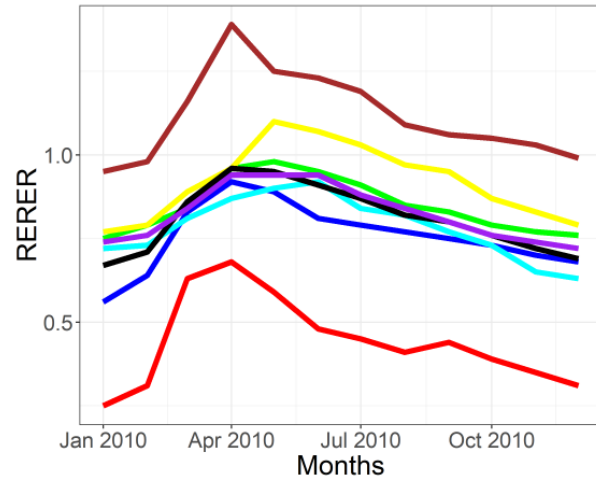
985

986

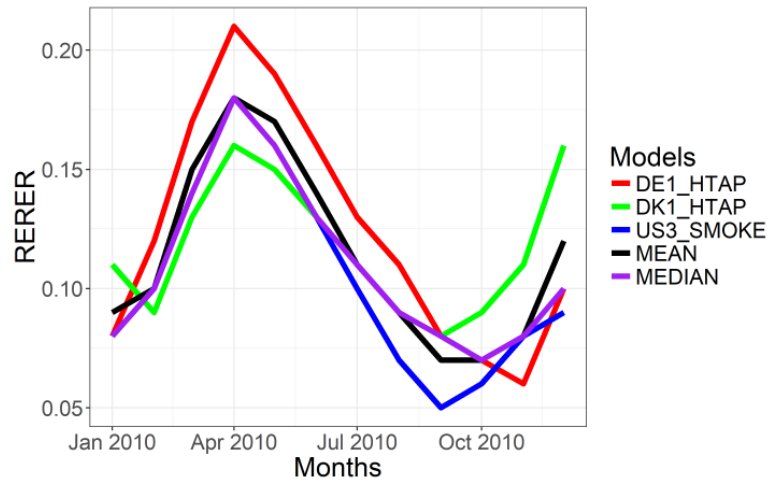
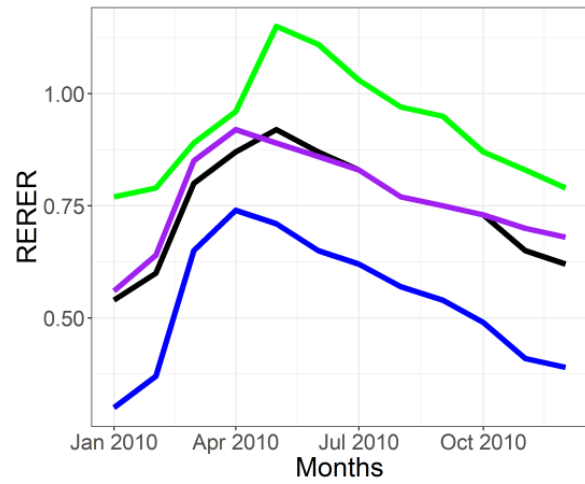
Fig. 17. Spatial distribution of RERER values constructed from the annual mean responses of O_3 and $PM_{2.5}$ over Europe and North America.

Formatted: Subscript

Formatted: Subscript



- Models**
- DE1_HTAP
 - DK1_HTAP
 - FI1_MACC
 - FR1_HTAP
 - IT1_MACC
 - UK1_MACC
 - MEAN
 - MEDIAN



- Models**
- DE1_HTAP
 - DK1_HTAP
 - US3_SMOKE
 - MEAN
 - MEDIAN

Fig. 18. Seasonal variations of RERER values of O₃ and PM_{2.5} over Europe and North America.

Formatted: Subscript

Formatted: Subscript